Deep-Sea Research II 71-76 (2012) 77–93

Contents lists available at SciVerse ScienceDirect

Deep-Sea Research II

journal homepage: www.elsevier.com/locate/dsr2

Spatial distribution of pCO_2, $\Delta O_2/Ar$ and dimethylsulfide (DMS) in polynya waters and the sea ice zone of the Amundsen Sea, Antarctica

Philippe D. Tortell [a,b,*], Matthew C. Long [c], Christopher D. Payne [a], Anne-Carlijn Alderkamp [d], Pierre Dutrieux [e], Kevin R. Arrigo [d]

[a] Department of Earth and Ocean Sciences, University of British Columbia, 2146 Health Sciences Mall, Vancouver BC, Canada V6T 1Z3
[b] Department of Botany, University of British Columbia, 6270 University Blvd., Vancouver BC, Canada V6T 1Z4
[c] National Center for Atmospheric Research, 1850 Table Mesa Drive, Boulder, CO 80305, USA
[d] Department of Environmental Earth Systems Sciences, Stanford University, 473 Via Ortega, Stanford, CA 94305, USA
[e] Physical Science Division, British Antarctic Survey, High Cross Madingley Road, Cambridge CB3 0ET, United Kingdom

ARTICLE INFO

Available online 16 March 2012

Keywords:
Amundsen Sea
pCO_2
O_2/Ar
Dimethylsulfide
Iron
Phaeocystis
Diatoms
Net community production
Air–sea exchange
Modified circumpolar deep water

ABSTRACT

We report the first simultaneous measurements of surface water pCO_2, biological oxygen saturation ($\Delta O_2/Ar$) and dimethylsulfide (DMS) concentrations in polynya waters and the sea ice zone of the Amundsen Sea, Antarctica. Across our survey region, we observed large spatial variability in surface water gas concentrations, tied to strong gradients in hydrography and phytoplankton biomass. Variability in sea surface temperature and salinity was attributed to the interacting effects of surface ocean circulation and heat fluxes, sea ice melt and the upwelling of relatively warm, saline and nutrient-rich modified circumpolar deep water. Phytoplankton biomass ranged from $<1\ \mu g\ L^{-1}$ to $\sim 40\ \mu g\ L^{-1}$ chlorophyll *a* (Chl *a*), with the highest values observed in regions of shallow mixed layer depths. Phytoplankton assemblages were dominated by the colonial haptophyte *Phaeocystis antarctica* at most sampling stations, with lesser abundances of diatoms found throughout the polynya and sea ice zone. Cryptophytes were abundant at a few stations along the continental shelf break. Across the open polynya waters and sea ice zone, $\Delta O_2/Ar$ ranged from $\sim -40\%$ to 40% (mean 8.6%), pCO_2 ranged from 80 to 530 μatm (mean 250 μatm) and DMS concentrations varied from <1 nM to ~ 350 nM. Strong gradients in gas concentrations were observed over short (*i.e.* <10 km) spatial scales. The distribution of pCO_2 and $\Delta O_2/Ar$ across our survey transects reflected the balance between deep water entrainment and net community production, with a significant imprint of air–sea exchange. Chl *a* concentrations were significantly correlated to both pCO_2 and $\Delta O_2/Ar$, and the slope of the $\Delta O_2/Ar$ *vs.* pCO_2 relationship was consistent with photosynthetic stoichiometry (~ 1.25 mol O_2 evolved per mol DIC removed). DMS and Chl *a* concentrations were also correlated in surface waters, but the spatial distribution of DMS was often uncoupled from pCO_2 and $\Delta O_2/Ar$, likely due to complex microbial cycling processes. Sea surface temperature and salinity were related to surface gas concentrations through their effects on mixed layer depth and as tracers of upwelling. During the time of our cruise, the Amundsen Sea acted as an overall net sink for CO_2 (mean sea–air flux $= -15.9$ mmol $m^{-2}\ d^{-1}$) and a DMS source (mean sea–air flux $= 23.1$ μmol $m^{-2}\ d^{-1}$). Sea–air CO_2 and DMS fluxes were more than 2-fold higher in open polynya waters relative to the overall cruise means. Simple calculations suggest that the Amundsen Sea contributes $\sim 5\%$ of total Southern Ocean CO_2 fluxes, and $\sim 1\%$ of DMS fluxes.

1. Introduction

Antarctic continental shelf seas exert a strong influence on Southern Ocean biogeochemical cycles (Marinov et al., 2006; Arrigo et al., 2008) despite accounting for less than 10% of the surface area in this vast oceanic region. Unlike much of the Southern Ocean (south of 50°S), which experiences chronic Fe limitation (Boyd, 2002), coastal polynyas (seasonally open waters surrounded by permanent sea ice cover) receive Fe inputs from melting sea ice and continental shelf sediments (Sedwick and DiTullio, 1997; Coale et al., 2005). As a result, primary productivity in these systems can exceed $2\ g\ C\ m^{-2}\ d^{-1}$, accounting for $\sim 40\%$ of total Southern Ocean C-fixation (Arrigo et al., 1998; Arrigo and van Dijken, 2003). High primary productivity in polynya surface waters lowers the partial pressure of CO_2 below

* Corresponding author at: Department of Earth and Ocean Sciences, University of British Columbia, 2146 Health Sciences Mall, Vancouver BC, Canada V6T 1Z3. Tel.: +604 822 4728; fax: +604 822 6091.
E-mail address: ptortell@eos.ubc.ca (P.D. Tortell).

0967-0645/$ - see front matter © 2012 Elsevier Ltd. All rights reserved.
doi:10.1016/j.dsr2.2012.03.010

atmospheric saturation (Sweeney et al., 2000; Arrigo et al., 2008), driving an influx of CO_2 and the subsequent export of particulate and dissolved organic C into subsurface waters (Dunbar et al., 1998). The global impact of this biological C pump is enhanced by the formation of deep water masses over the Antarctic continental shelf (Jacobs, 2004), which carry carbon into the ocean interior and sequester CO_2 from the atmosphere on 100–1000 year timescales (Marinov et al., 2006). Sea ice formation impedes sea–air exchange with pCO_2 supersaturated polynya waters during winter (Gibson and Trull, 1999; Sweeney, 2003; Arrigo and Van Dijken, 2007), ensuring that these regions are a net sink for CO_2 on annual timescales (Arrigo et al., 2008).

Beyond their contribution to the Southern Ocean C cycle, Antarctic polynya waters also exhibit extremely high concentrations and sea–air fluxes of the climate-active trace gas dimethylsulfide (DMS, DiTullio and Smith, 1995; Zemmelink et al., 2005; Kiene et al., 2007; Tortell et al., 2011). This compound is derived from the algal metabolite dimethylsulfoniopropionate (DMSP), and cycled through the marine foodweb (Simo, 2004; Stefels et al., 2007). Oceanic DMS emissions are a significant source of atmospheric sulfur aerosols (Bates et al., 1992), which backscatter incoming solar radiation, enhance cloud formation and thus increase Earth's albedo (Thomas et al., 2010). It has been suggested that the biological production of DMS in marine surface waters may act as a climate feedback mechanism (Charlson et al., 1987). If such a DMS-climate feedback exists, the Southern Ocean, by virtue of its vast surface area and high DMS concentrations (Lana et al., 2011), is likely to play a critical role. Indeed, several recent modeling studies have predicted changes in Southern Ocean DMS fluxes under global warming scenarios ($2\times$ CO_2), associated with changes in mixed layer stratification and phytoplankton species distributions (Bopp et al., 2004; Cameron-Smith et al., 2011). These predicted changes in Southern Ocean DMS concentrations could lead to significant global cooling and, thus, a negative climate feedback as proposed by Charlson et al. (1987).

Much of our understanding of the biogeochemical dynamics of Antarctic polynyas comes from extensive field studies in a few systems, most notably the Ross Sea and the Weddell Sea. In these regions, primary productivity increases rapidly during the Austral spring (late October/early November) in association with sea ice retreat, increasing solar irradiance and mixed layer stratification (Arrigo and van Dijken, 2003). Early season phytoplankton blooms in the Ross Sea are dominated by the colonial haptophye *Phaeocystis antarctica* under conditions of deep mixing, while diatoms become increasingly prevalent later in the growing season, particularly in highly stratified regions with significant meltwater inputs (DiTullio and Smith, 1996; Arrigo et al., 2000; Smith et al., 2000). During the height of the summertime bloom, pCO_2 of $\sim$100 μatm is observed in the most stratified waters (Bates et al., 1998; Sweeney et al., 2000; Tortell et al., 2011). These pCO_2 levels are among the lowest recorded in the world's oceans (Takahashi et al., 2009). Similarly extreme DMS concentrations ($>$50 nM) have been observed in the Ross and Weddell Sea polynyas, most notably during early springtime *P. antarctica* blooms (Ditullio and Smith, 1995; Kiene et al., 2007; Tortell et al., 2011) and in regions of sea ice melt (Zemmelink et al., 2005).

At present, the extent to which the biogeochemical characteristics of the Ross and Weddell Seas are representative of other Antarctic polynyas is largely unknown due a paucity of relevant field data. Our current understanding of polynya dynamics comes mostly from satellite observations of sea ice cover and surface Chl *a* concentrations. Using a remote sensing approach, Arrigo and van Dijken (2003) identified 37 distinct coastal Southern Ocean polynyas that exhibited substantial variability in the magnitude and seasonal cycle of phytoplankton blooms. Among all the polynyas identified, the highest Chl *a* concentrations and inferred C-fixation rates were located in two adjacent regions of the Amundsen Sea; the Amundsen and Pine Island polynyas. On an areal basis, these polynyas appear to be the most biologically productive regions in the entire Southern Ocean (Arrigo and van Dijken, 2003), yet very little information is available on their biogeochemical characteristics. To date, most studies in the Amundsen Sea have focused on examining the rapid retreat of the West Antarctic Ice Sheet, in relation to the upwelling of warm Circumpolar Deep Water (CDW) onto the Antarctic continental Shelf (Thomas et al., 2004; Walker et al., 2007; Thoma et al., 2008; Wåhlin et al., 2010). Increased glacial melting in this region has been accompanied by a general freshening of surface waters along the Antarctic margin (Jacobs and Giulivi, 2010), with significant implications for surface ocean circulation, phytoplankton productivity and biogeochemical cycles.

In this article, we present new field data examining the surface water distribution of DMS, pCO_2 and $\Delta O_2/Ar$ within the polynya and beneath the pack ice of the Amundsen Sea, using ship-board membrane inlet mass spectrometry (MIMS) for high spatial resolution analysis. $\Delta O_2/Ar$ provides a tracer for net biological O_2 cycling, since Ar normalization largely removes the effects of physical processes (*e.g.* temperature changes and bubble injection) on O_2 saturation states (Craig and Hayward, 1987). Our research objective was to document the spatial variability of mixed layer gas concentrations and sea–air fluxes in relation to underlying physical and biological variables such as sea ice cover, surface hydrography, and phytoplankton biomass and taxonomic composition. Our results provide new insight into the biogeochemistry of the Amundsen Sea, demonstrating extreme pCO_2 drawdown, DMS accumulation and biologically-induced O_2 supersaturation that is consistent with the exceptionally high primary productivity of this system. Furthermore, our high-resolution measurements allow us to document large variability in surface water gases over short spatial scales. We compare our results with recently published MIMS data from the Ross Sea (Tortell et al., 2011), to examine the similarities and differences in surface water gases between these two polynya systems.

2. Methods

2.1. Dissolved gas concentrations and sea–air fluxes

Continuous underway gas data were collected in the Amundsen Sea (Fig. 1) from January 11 to February 16, 2009 on board the RV/IB *Nathanial B. Palmer* (cruise NBP 09-01) as part of the DynaLiFe program. The cruise track covered the pack ice zone situated over the continental shelf break (1500 m isobath) and the Pine Island and Amundsen polynyas (hereafter abbreviated as PIP and AP, respectively). A significant portion of our cruise was dedicated to a detailed survey of the waters adjacent to the Pine Island Glacier (PIG). Samples were collected from the ship's uncontaminated seawater supply at a nominal depth of $\sim$5 m. Surface water pCO_2, DMS and $\Delta O_2/Ar$ were measured with high frequency (several times per minute) using membrane inlet mass spectrometry (MIMS), following the procedures described in detail elsewhere (Tortell, 2005; Tortell et al., 2011). DMS and $\Delta O_2/Ar$ calibrations were conducted using seawater standards as described by Tortell et al. (2011). Because CO_2 standards were unavailable for the MIMS during our voyage, the MIMS CO_2 measurements were calibrated against the pCO_2 data derived from the Lamont–Doherty NDIR equilibrator system installed on the *N.B. Palmer* (Takahashi et al., 2000; http://www.ldeo.columbia.edu/res/pi/CO2/carbondioxide/Palmer_data/0901SFC.PRT).
The Lamont–Doherty NDIR was calibrated every six hours using four CO_2 standard gas mixtures prepared by CMDL/NOAA, and the data are reported at *in situ* sea surface temperature. Raw MIMS

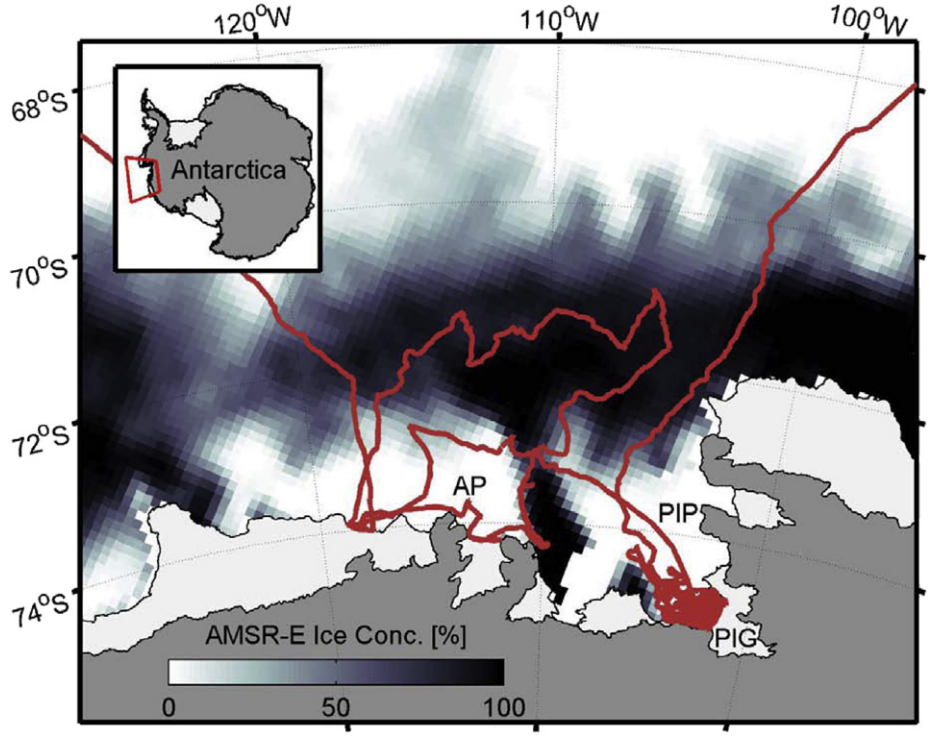

Fig. 1. Map of the ship's cruise track (red line) superimposed on the mean sea ice concentration during the period of our survey (Jan. 11–Feb. 16, 2009). Dark gray areas represent the Antarctic continent, while light gray areas represent land fast ice and glaciers. AP, PIP and PIG represent the locations of the Amundsen Polynya, Pine Island Polynya and Pine Island Glacier, respectively. The inset map shows the location of the study area (red box) relative to the Antarctic continent. (For interpretation of the references to color in this figure legend, the reader is referred to the web version of this article.)

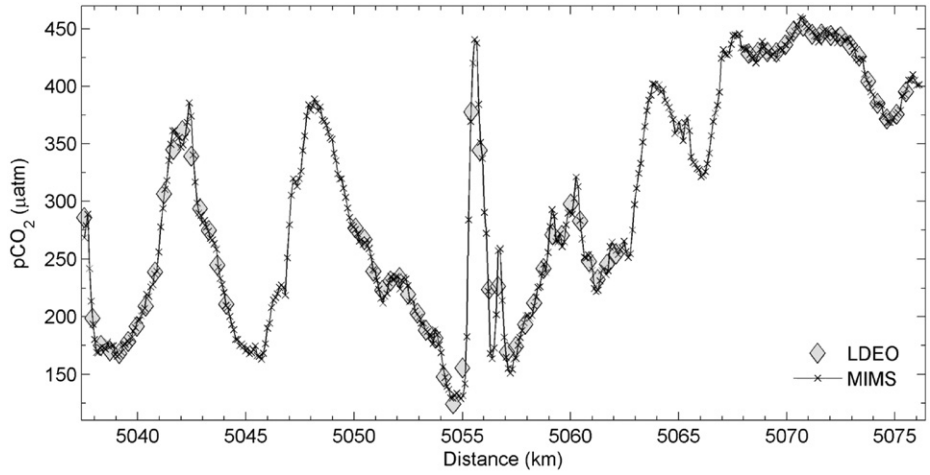

Fig. 2. Comparison of underway MIMS pCO_2 measurements with data obtained from the LDEO equilibrator system. The figure demonstrates the excellent agreement between calibrated MIMS and LDEO measurements and the very high temporal resolution of the MIMS data.

CO_2 measurements (ion current at mass/charge ratio of 44) were aligned to the LDEO equilibrator data using linear regression ($r^2=0.97$, $n=145{,}790$). While the MIMS and the LDEO equilibrator data showed very similar patterns of pCO_2 variability across our survey region, the MIMS data have the advantage of higher spatial resolution, and fewer data gaps associated with extended calibration sequences during underway transit. Fig. 2 shows an example of the tight coherence between MIMS and LDEO pCO_2 data, and the higher sampling resolution of the MIMS measurements. Such high resolution presents a significant advantage in spatially heterogeneous waters.

We used our surface concentration measurements and wind speed data to calculate sea–air fluxes for CO_2 and DMS. We computed sea–air exchange of CO_2 as

$$F_{CO_2} = (1-A)k_{CO_2}\gamma(pCO_{2sw}-pCO_{2atm}) \quad (2)$$

where A is the fraction of sea surface covered by ice, γ is the temperature and salinity-dependent solubility of CO_2 (Weiss, 1974), and k_{CO_2} is the gas transfer velocity ($m\,d^{-1}$), calculated as a function of instantaneous wind speed and the temperature-dependent Schmidt number (Wanninkhof, 1992). Wind speed data were derived from the ship's anemometer, while sea ice concentrations were obtained from the AMSR-E satellite product (Cavalieri et al., 2004) with a spatial resolution of 12.5 km. We assume a constant value for pCO_2 atm of 372 µatm derived from the GlobalView atmospheric CO_2 database (http://www.esrl.

noaa.gov/gmd/ccgg/globalview/), and a mean atmospheric pressure (measured by the ship's meteorological sensors) of 0.97 atm. For DMS, since atmospheric concentrations are often assumed to be negligible, we compute sea–air flux as

$$F_{DMS} = (1-A)k_{DMS}(DMS_{sw}) \quad (3)$$

where DMS_{sw} is the concentration of DMS in the surface ocean and k_{DMS} is the gas transfer velocity derived from the equations of Wanninkhof (1992) for instantaneous wind speeds, normalized to the DMS Schmidt number of Saltzman et al. (1993). Recent work has suggested that the Wanninkhof (1992) formulation may overestimate the gas transfer velocity for DMS at wind speeds above 10 m s^{-1} (Vlahos and Monahan, 2009) and our sea–air fluxes may thus represent upper bounds in regions of high wind speed. Nonetheless, we use this calculation scheme in order to compare Amundsen Sea DMS fluxes with those computed recently from MIMS data in the Ross Sea (Tortell et al., 2011). In contrast, our flux estimates may overestimate if atmospheric DMS concentrations are not negligible, as we have assumed. Unfortunately, atmospheric measurements of DMS are not available from our cruise.

We computed the sea–air flux of CO_2 and DMS using surface water gas concentrations, wind speeds and Schmidt numbers binned to a spatial resolution of 12.5 km, corresponding to the grid size of the AMSR-E sea ice data. This binning procedure was employed to decrease the relative weighting of highly sampled regions of our cruise track, thus making our polynya-wide averages more spatially representative.

2.2. Hydrographic data and phytoplankton biomass

Measurements of SST (~5 m) and salinity were logged continuously from the ship's thermosalinograph (SeaBird, Model SBE-21), while sea surface Chl *a* fluorescence (used as a proxy for bulk phytoplankton biomass) was continuously recorded by the ship's underway fluorometer (Turner, 10-AU-005). These underway measurements were aligned with MIMS data using GPS timestamps. Total phytoplankton biomass and taxonomic composition were also assessed using fluorometry and HPLC analysis of Chl *a* and accessory photosynthetic pigment concentrations determined in discrete surface water samples (10 m depth) at 51 stations. These samples were collected using GO-FLO bottle casts. For Chl *a* analysis, seawater samples were filtered onto 25 mm GF/F filters, extracted overnight in 90% acetone and analyzed on a Turner Design fluorometer as described by Welschmeyer (1994). Samples for additional pigment measurements were collected on glass fiber filters (GF/F, nominal pore size 0.7 μm), flash frozen in liquid N_2 and returned to the laboratory for subsequent analysis. In the laboratory, pigments were extracted in 90% acetone for at least 24 h at 4 °C and quantified using the method described by Alderkamp et al. (2012). We used diagnostic pigments to assess the taxonomic composition of phytoplankton, employing the CHEMTAX algorithm (Mackey et al., 1996), as described by Alderkamp et al. (2012). Additional information on surface water Chl *a* concentrations was obtained from level 3 processed MODIS-Aqua imagery (http://oceancolor.gsfc.nasa.gov/cgi/l3) using 8-day composite data to minimize cloud interference.

3. Results

3.1. Sea ice distributions and surface water hydrography

Our study area consisted of two distinct polynyas (Amundsen polynya; AP and Pine Island Polynya; PIP), separated by a region of sea ice (>75% ice cover) extending north from the Antarctic continent (Fig. 1). During the time of our survey, sea ice cover was <10% within both of these polynyas. The northern edge of the polynyas was defined by a ~2° latitudinal band of pack ice (>70% ice cover) situated over the continental shelf break (1500 m isobath). During the 2008–2009 Austral summer, the AP and PIP exhibited open water for ~145 days, reaching maximum sizes of 31,000 and 19,700 km^2, respectively, in early February (Arrigo et al., 2012). The temporal evolution of the 2008–2009 polynyas was typical of that observed over the 13 year historical record presented by Arrigo et al. (2012).

Across both polynya waters and the pack ice zone, surface water salinity ranged from 32.5 to 34.1, while SST ranged from −1.8 to 1.9 °C (Fig. 3). Surface warming and residual sea ice melt caused the temperature–salinity relationship of surface waters to depart from that of subsurface water masses, yielding significant scatter in the *T*–*S* diagram. Relatively cold (<−0.5 °C) low salinity (<33.4) surface water was observed across much of the offshore AP, and in the northwest portions of the PIP (Fig. 4B and C), indicative of a residual ice melt signal in these regions. In contrast, relatively high SST and high salinity waters were located throughout much of the PIP and to a lesser extent, along the southwest coast of the AP (Fig. 4B). Increased SST in these regions can be attributed to solar heating of the mixed layer and/or the influence of relatively warm modified circumpolar deep-water (MCDW, *T*~1.1 °C, *S*~34.7, Jacobs et al., 2011) outflow onto the continental shelf. The MCDW signature can be discerned in CTD depth profiles as a subsurface temperature maximum below the remnant winter water layer at ~300 m. Such a feature was apparent at a number of locations through our study site, most notably in the PIP, near the Pine Island Glacier (PIG), and adjacent to the Dotson and Crosson Ice shelves in the southwest AP (Alderkamp et al., 2012). In these regions, we observed evidence for the entrainment of MCDW into surface waters based on very high NO_3^- concentrations (>30 μm; Alderkamp et al., 2012), associated with low $\Delta O_2/Ar$ and high pCO_2 surface waters (see below).

Examination of CTD depth profiles showed significant variability in mixed layer stratification intensity across the polynya waters. Relatively weak vertical stratification and deep mixed

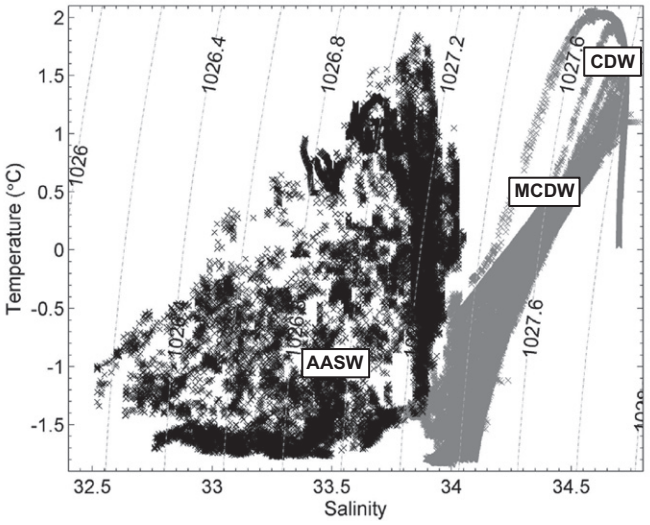

Fig. 3. Temperature *vs.* salinity diagram for surface (~5 m, black symbols) and sub-surface (>100 m, gray symbols) water masses in the Amundsen Sea. Deep water measurements were obtained from CTD casts, while surface data were obtained from the ship's underway thermosaliograph. Labeled contours represent calculated seawater density. Boxes denote the approximate *S* and *T* characteristics corresponding to Antarctic Surface Water (AASW), Modified Circumpolar Deep Water (MCDW) and Circumpolar Deep Water (CDW).

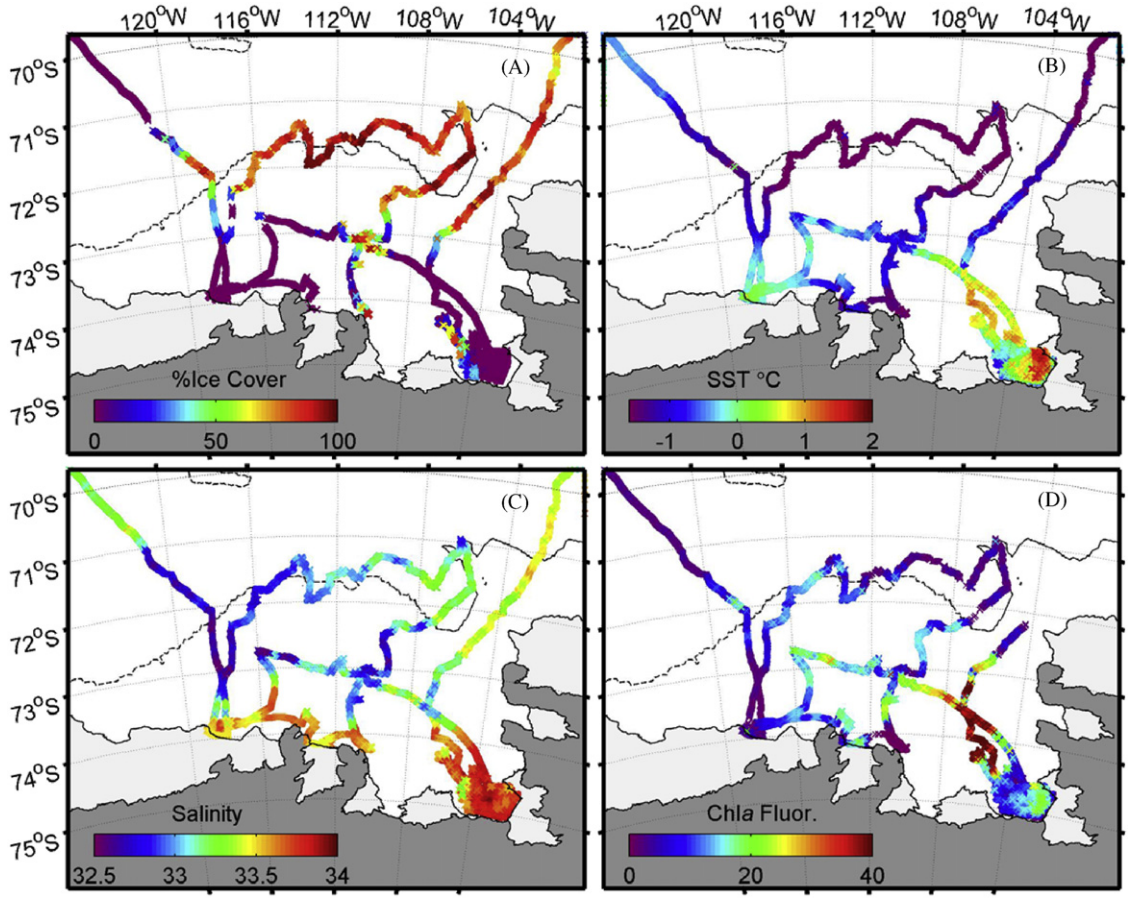

Fig. 4. Spatial distribution of (A) AMSR-E derived sea ice cover, (B) sea surface temperature (SST), (C) salinity and (D) Chl *a* fluorescence along the ship track in the Anumdsen Sea. Dark gray and light gray shaded areas represent the Antarctic continent and land fast ice, respectively. The dashed gray line represents the location of the 1000 m isobath.

layer depths were observed at a number of stations, most prominently in regions of inferred MCDW outflow adjacent to the PIG, and the Crosson and Dotson ice shelves in the AP. In contrast, local surface freshening and warming resulted in shallow mixed layers in the central region of both the AP and PIP. Across our entire survey region, mixed layer depths, calculated using a density difference criterion ($\Delta\sigma_t$) of 0.05 kg m^{-3}, ranged from 9 to 160 m with a median value of 28 m and a mean of 44 $\pm$ 37 (std. dev.).

3.2. Phytoplankton biomass and taxonomic composition

Examination of MODIS-Aqua 8-day composite imagery during the 2008–2009 Austral summer showed that our sampling period corresponded with the seasonal maximum in Chl *a* concentrations in the Amundsen Sea (Arrigo et al., 2012). For both the AP and PIP, mean Chl *a* concentrations began increasing sharply in mid-December, reaching maximum values of ~6 μg L^{-1} near the beginning of our survey in mid-January. During the last two weeks of our cruise, satellite-derived Chl *a* concentrations dropped significantly, with mean concentrations of ~2 μg L^{-1}. The mean Chl *a* values and the temporal dynamics of the 2008–2009 phytoplankton blooms were consistent with the 13 year climatology compiled by Arrigo et al. (2012). This indicates that we sampled the Amundsen Sea polynyas under 'typical' summertime conditions of peak phytoplankton biomass and initial bloom termination.

During our cruise, surface water (< 10 m) Chl *a* concentrations measured at discrete sampling stations ranged from ~0.3 to 10.9 μg L^{-1}, with a mean value of 3.4 $\pm$ 2.6 μg L^{-1}. Chl *a* fluorescence, measured continuously by the ship's underway sensors, was strongly correlated to the discrete surface Chl *a* measurements (r^2=0.80, p < 0.001, n=28), justifying the use of underway fluorescence as a high spatial resolution Chl *a* proxy along the ship's track. However, the higher resolution of surface water fluorescence measurements enabled us to capture a larger dynamic range in phytoplankton biomass than was apparent in discrete samples. The lowest Chl *a* values inferred from fluorescence (< 0.1 μg L^{-1}) were observed in the pack ice zone and in regions of assumed MCDW outflow adjacent to the PIG and along coastal sections of the AP (Fig. 4D). Chl *a* fluorescence was highest (> 40 μg L^{-1}) in the central waters of PIP, NW of the PIG, in association with relatively high SST and shallow mixed layer depths. High surface Chl *a* fluorescence (> 10 μg L^{-1}) was found exclusively in regions of relatively shallow (< 30 m) mixed layers (Fig. 5). There was, however, only a weak relationship between mixed layer depth and surface Chl *a* (r^2=0.21) across our full survey region.

Diatoms and *P. antarctica* were the dominant phytoplankton taxa in both the open polynya waters and beneath the pack ice, accounting for an average of 93% of the total Chl *a* concentrations (based on CHEMTAX analysis; Alderkamp et al., 2012). At the majority of our sampling stations, phytoplankton assemblages were dominated by *P. antarctica*. This species accounted for more than 66% of the total Chl *a* at 29 of the 44 stations we sampled and was also present in significant abundances (between 33% and 66% of total Chl *a*) at a further 9 stations (Fig. 6). *P. antarctica* abundance was high throughout both the AP and PIP (Fig. 6), with a significant fraction of the biomass associated with colonies. In contrast, diatoms dominated the phytoplankton assemblages (> 66% of the total Chl

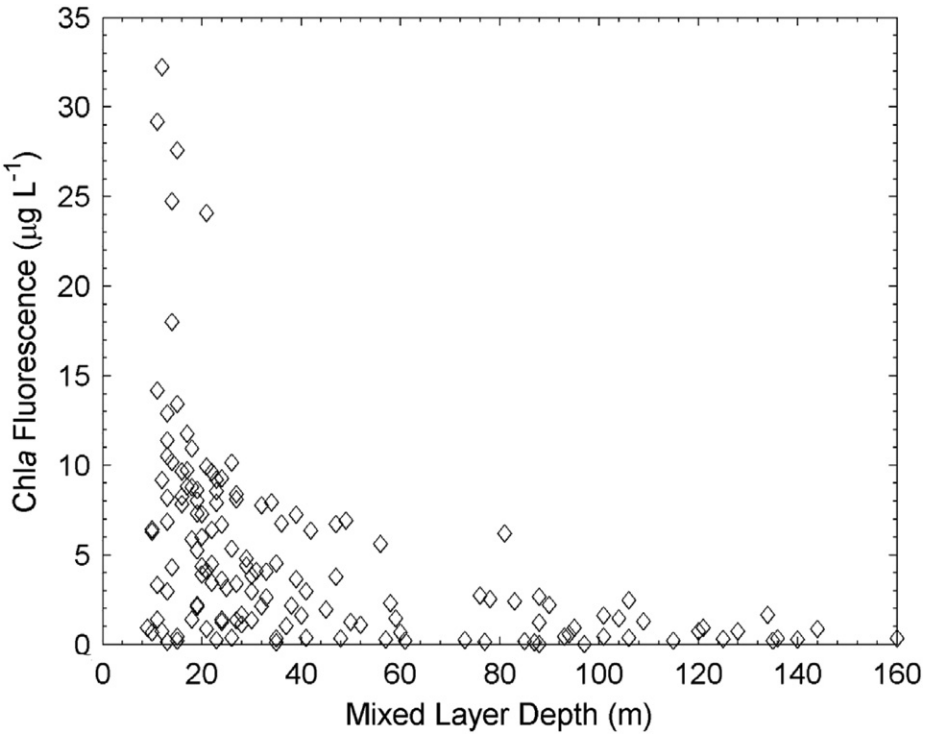

Fig. 5. Relationship between surface water (<10 m) Chl *a* fluorescence and mixed layer depth, computed using a density difference criterion of 0.05 kg m^{-3}.

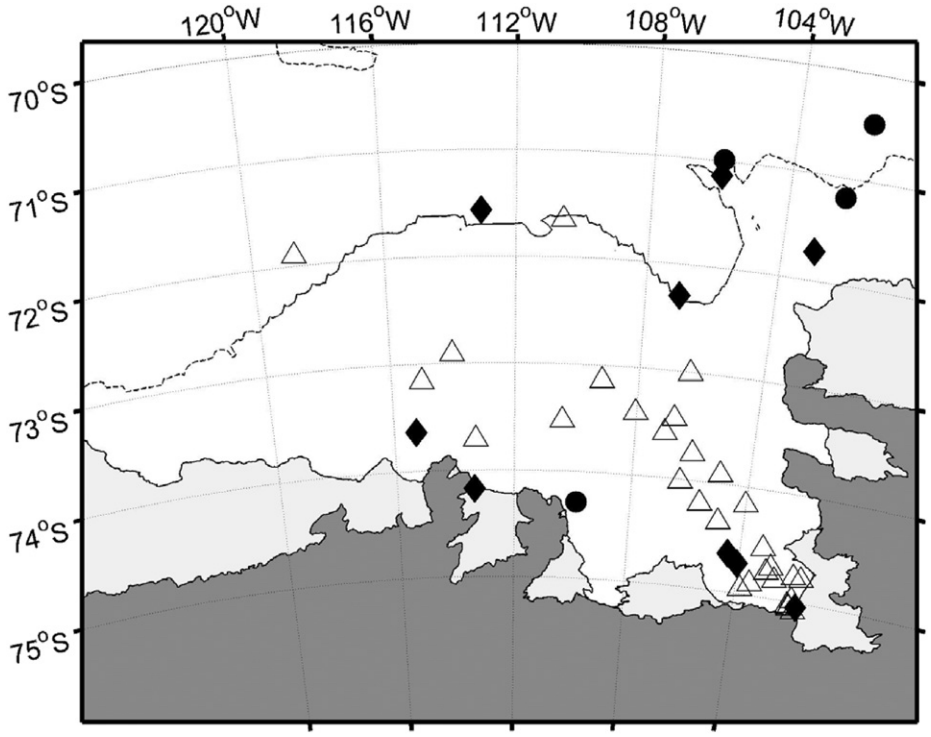

Fig. 6. Spatial distribution of phytoplankton taxa across our survey region. Hollow triangles represent stations where *P. antarctica* accounted for more than 66% total Chl *a* concentrations; filled circles represent diatom-dominated stations ($>66\%$ Chl *a* concentrations) and filled diamonds represent stations with where diatoms and *P. antarctica* represent $>33\%$ and $<66\%$ of total phytoplankton biomass. Taxonomic composition was assessed using CHEMTAX analysis of photosynthetic pigment concentrations in the upper 10 m.

a) at only 4 stations and accounted for $<33\%$ of phytoplankton biomass at 33 stations. The relative abundance of diatoms was greatest near the coast and in the pack ice over the continental shelf break (Fig. 6). In these regions, however, total phytoplankton biomass, and thus the absolute abundance of diatoms, was low. At several pack ice stations, cryptophytes and chlorophytes were also well represented in the phytoplankton assemblages, contributing up to $\sim$40% of the total Chl *a* (Fig. 6).

3.3. Surface gas concentrations

Across our sampling region, we observed high variability in surface water $\Delta O_2/Ar$, pCO_2 and DMS (Fig. 7). For the full data set, including open waters and ice covered regions, $\Delta O_2/Ar$ ranged from -40% to 43%, with a mean of $8.6 \pm 16.6\%$ (Fig. 7A), while pCO_2 ranged from 84 to 560 μatm, with a mean value of 251 ± 105 μatm (Fig. 7C). DMS concentrations varied by more than two orders of magnitude (<1 nM to $\sim$350 nM) and exhibited a positively skewed frequency distribution. The mean and median DMS concentrations were 36 and 16 nM, respectively, with a standard deviation and inter-quartile range (*i.e.* difference between the 75th and 25th percentile) of 54 and 25 nM (Fig. 7E). Within our overall sampling region, a clear distinction was evident between open polynya waters, pack ice, and the Southern Ocean pelagic zone north of the continental shelf (Fig. 7B, D, and F). Compared to the pack ice and polynya waters, the pelagic zone showed relatively little variability in surface gas concentrations, with $\Delta O_2/Ar$ and pCO_2 close to atmospheric equilibrium and DMS levels generally below $\sim$5 nM. In contrast, $\Delta O_2/Ar$ was supersaturated in virtually all of the polynya waters (range 0–40%), while pCO_2 was undersaturated (range $\sim$100–300 μatm) and DMS generally exceeded 10 nM. Gas concentrations in the pack ice showed a multi-modal distribution for all gases, possibly reflecting heterogeneity in sea ice cover and differing productivity levels within leads *versus* ice covered-waters. Indeed, there was a weak positive (negative) correlation between 12.5 km resolution sea ice cover and pCO_2 ($\Delta O_2/Ar$) in the pack ice domain ($r \sim 0.4$).

Beyond the broad differences between the pelagic zone, pack ice, and polynya waters, we observed other significant spatial gradients in gas concentrations (Fig. 8). In particular, there was a strong productivity signal (high $\Delta O_2/Ar$, low pCO_2) associated with high Chl *a* concentrations in the stratified waters of the northwest PIP (Fig. 8A and C). In this region, maximum $\Delta O_2/Ar$ exceeded 40% while the minimum pCO_2 was $\sim$80 μatm. DMS concentrations were also highest in this region, with maximum values exceeding 300 nM (Fig. 8D). In contrast, we observed high pCO_2 and negative $\Delta O_2/Ar$ close to the PIG and along the southeast coast of the AP. The low $\Delta O_2/Ar$ and high pCO_2 likely reflect a remnant net heterotrophic signature that is indicative of MCDW upwelling, rather and net heterotrophy in surface waters *per se*.

Repeated sampling in Pine Island Bay (PIB) allowed us to map the distribution of gases in this region with particularly high spatial resolution (Fig. 9). This detailed survey revealed extreme concentration gradients over small spatial scales. The apparent effect of upwelling (high pCO_2 and low $\Delta O_2/Ar$) was confined to a narrow band along the face of the PIG in the eastern portion of PIB. In close proximity to these upwelled waters, we observed a large biological productivity signal with $\Delta O_2/Ar$ values of $\sim$40% and pCO_2 of $\sim$100 μatm (Fig. 9A and C). This high productivity signal was concentrated in the northeast corner of PIB, associated with the highest SST waters of the entire survey region (Fig. 9D). DMS concentrations also showed high spatial variability in PIB, although the spatial distribution of this gas was different than that of pCO_2 and $\Delta O_2/Ar$ (Fig. 9E). The highest DMS concentrations in this region ($\sim$130 nM) were observed south

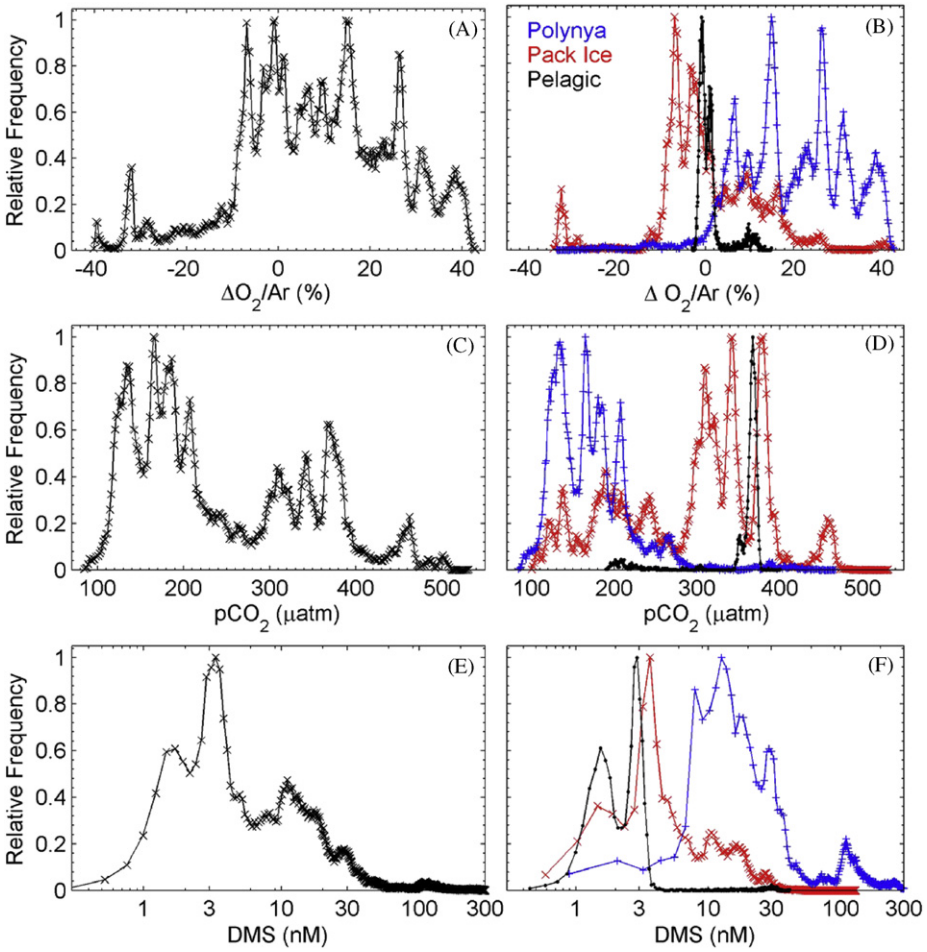

Fig. 7. Frequency distribution of pCO_2, $\Delta O_2/Ar$ and DMS across our full survey region (panels A, C, E), and for individual sampling domains (panels B, D, F). All frequencies are normalized to a maximum value of 1 to facilitate comparisons between the subplots. Note the logarithmic *x* scaling on panels (E) and (F).

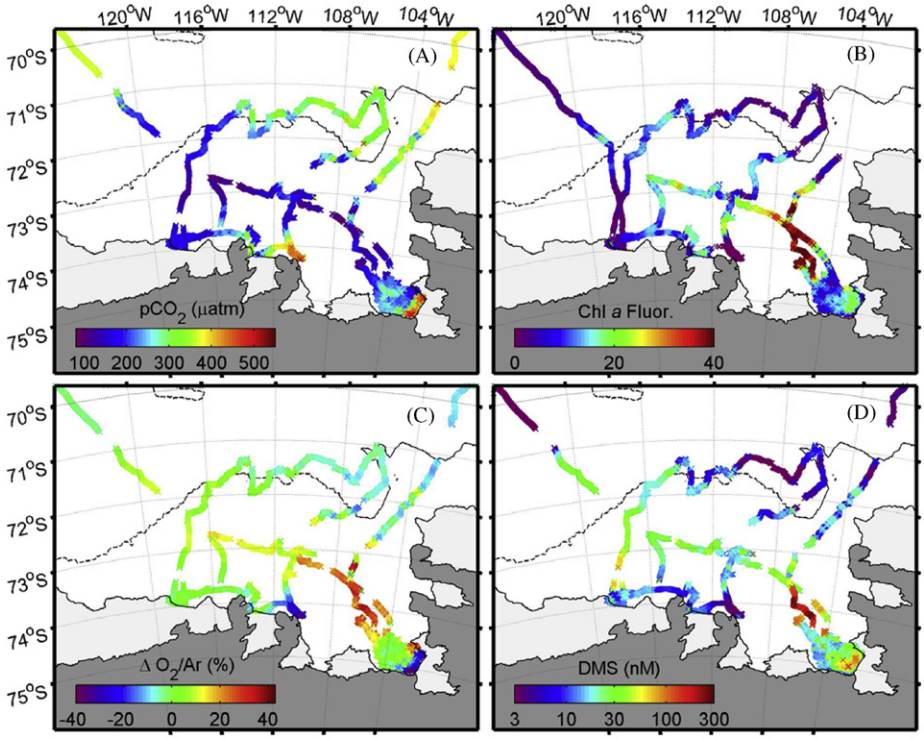

Fig. 8. Spatial distribution of pCO_2 (A), Chl *a* fluorescence (B), $\Delta O_2/Ar$ (C) and DMS (D) across our survey region. Note the logarithmic scaling used for DMS concentrations.

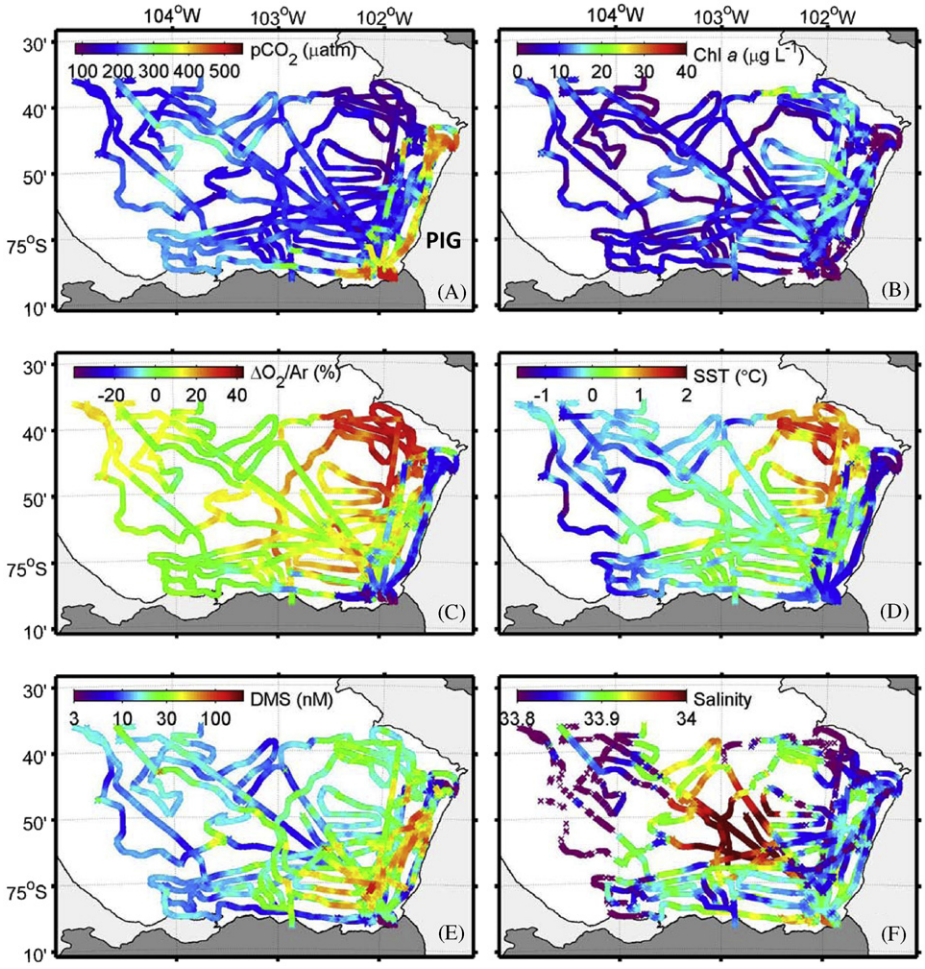

Fig. 9. Gas and hydrographic distributions in the vicinity of the Pine Island glacier (PIG). Dark gray and light gray shaded areas represent the Antarctic continent and land fast ice/glaciers, respectively.

of the local maximum in apparent phytoplankton productivity (compare Fig. 9C and E).

The spatial variability that is apparent in Figs. 8 and 9 is more clearly illustrated in Fig. 10, which shows gas concentrations, Chl *a* fluorescence, SST, and sea ice concentrations plotted along the cruise track. Data collected before ~2200 km and after ~9000 km along the track are from the pelagic zone north of the pack ice. The transition across the ice pack into the polynya waters is clearly seen in the sharp departures in pCO_2 and $\Delta O_2/Ar$ from atmospheric equilibrium. Within the polynya waters, gas distributions exhibited extraordinary spatial variability. For example, on spatial scales of <10 km, we measured changes in pCO_2, $\Delta O_2/Ar$, and DMS of ~300 μatm, 70%, and 100 nM, respectively. We were able to resolve these striking spatial gradients with measurements every ~200 m along the cruise track.

The data presented in Fig. 10 suggest a tight coupling between pCO_2 and $\Delta O_2/Ar$ across our survey region. Indeed, these variables exhibited a strong negative relationship (Pearson correlation coefficient, $r=-0.87$) across the full transect (Table 1) and within the open polynya waters (Table 2). The relationship between pCO_2 and $\Delta O_2/Ar$ is plotted in Fig. 11, with salinity and wind speeds mapped on a color scale. For regions with relatively high salinity (>33.5 psu) and wind speeds of <10 m s^{-1}, the slope of

Table 1
Pearson correlation coefficients between underway measured parameters across our full survey region.

	Chl *a*	SST	Salinity	pCO_2	$\Delta O_2/Ar$	DMS
Chl *a*	1					
SST	0.59	1				
Salinity	0.11	0.68	1			
pCO_2	−0.60	−0.65	−0.07	1		
$\Delta O_2/Ar$	0.76	0.78	0.20	−0.87	1	
DMS	0.78	0.63	0.25	−0.47	0.66	1

Table 2
Pearson correlation coefficients between underway measured parameters for the polynya waters only.

	Chl *a*	SST	Salinity	pCO_2	$\Delta O_2/Ar$	DMS
Chl *a*	1					
SST	0.48	1				
Salinity	−0.22	0.39	1			
pCO_2	−0.51	−0.55	0.38	1		
$\Delta O_2/Ar$	0.74	0.78	−0.07	−0.75	1	
DMS	0.74	0.60	−0.02	−0.38	0.65	1

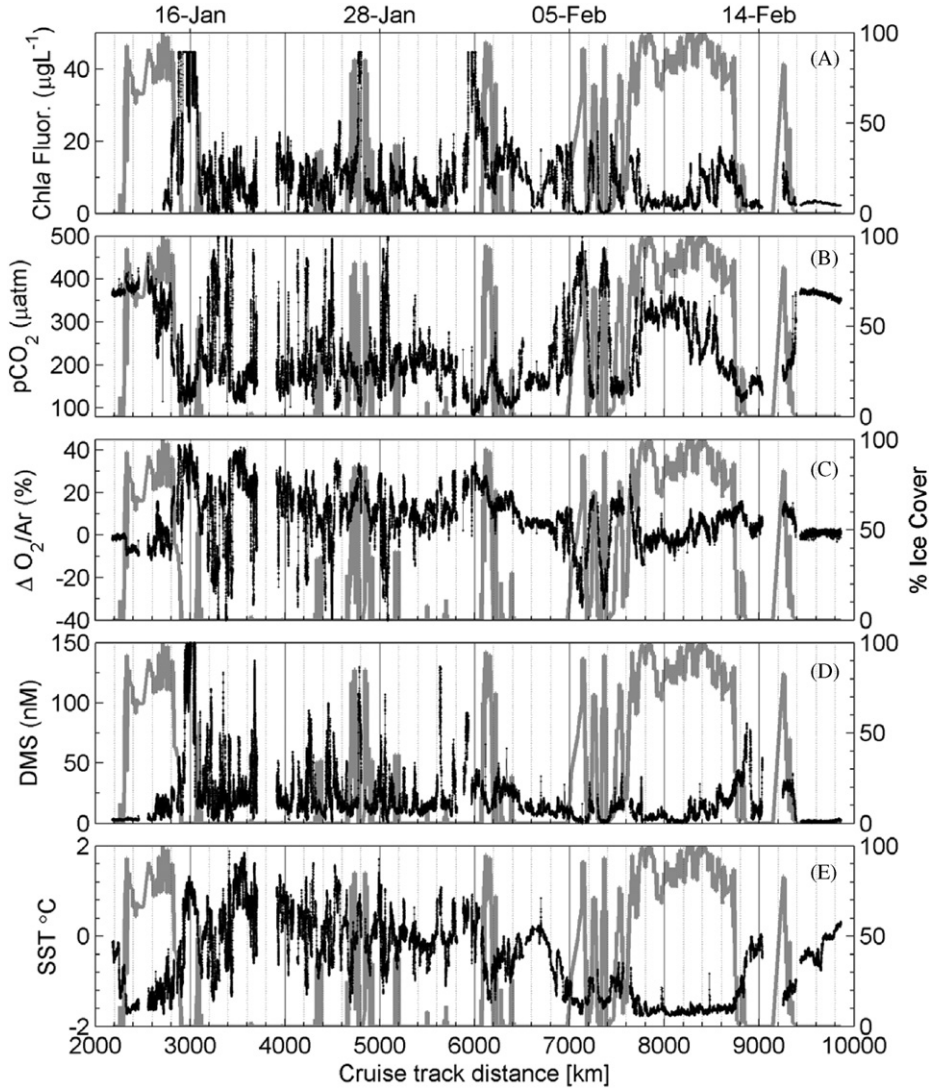

Fig. 10. Line plot of gases, sea surface temperature (SST) and Chl *a* as a function of cruise track distance. The gray line denotes AMSR-E-derived sea ice cover interpolated to the cruise track.

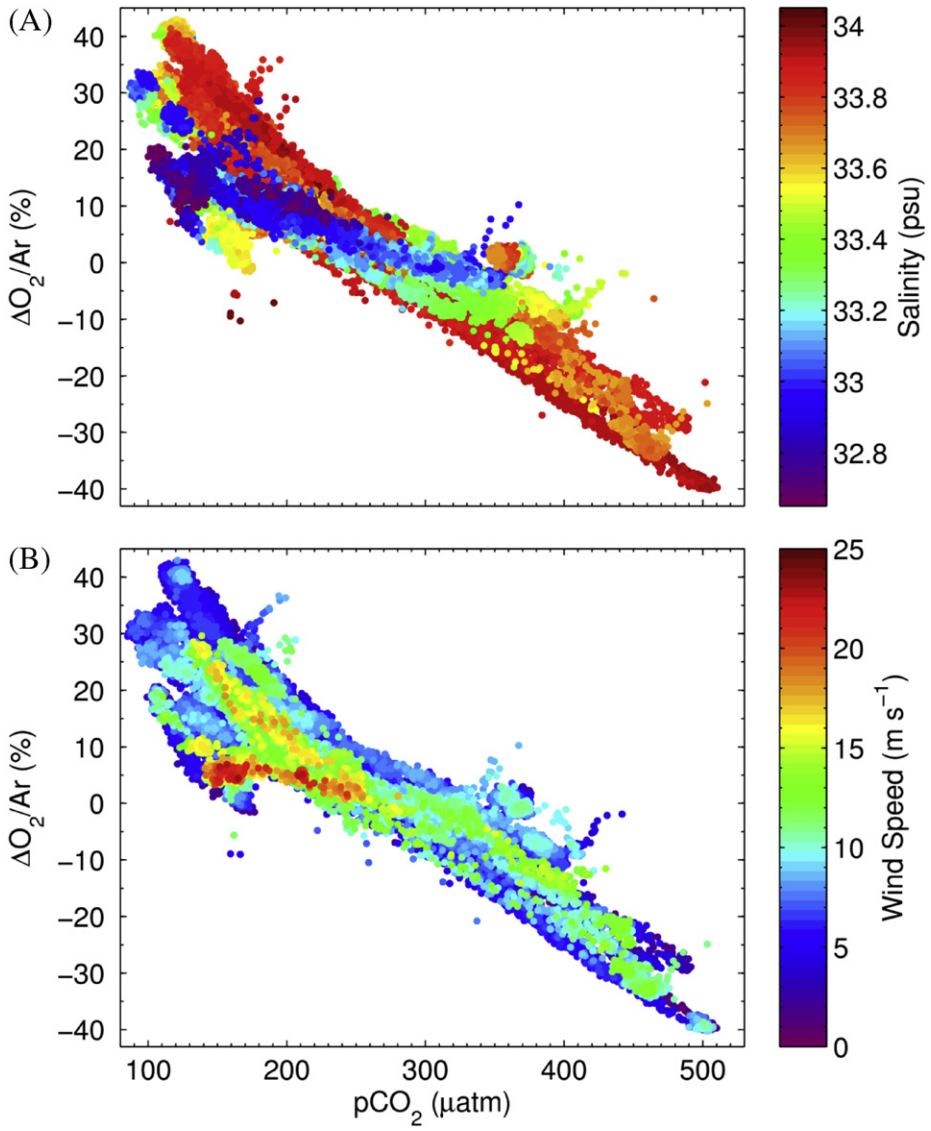

Fig. 11. Relationship between pCO_2 and $\Delta O_2/Ar$ for the full Amundsen Sea data set, with surface water salinity (A) and ship-derived wind speed (B) indicated on the color scale. (For interpretation of the references to color in this figure legend, the reader is referred to the web version of this article.)

the $\Delta O_2/Ar$ *vs.* pCO_2 relationship was -0.16. We converted the $\Delta O_2/Ar$ and pCO_2 measurements to O_2 and DIC concentrations using empirical relationships from the Ross Sea (Tortell et al., 2011) and estimated a slope of 1.25 (± 0.02) mol O_2 produced per mol DIC consumed in the high salinity (>33.5) surface waters of the Amundsen Sea. This value is in good agreement with typical photosynthetic quotients of 1.1–1.4 (Laws, 1991), indicating a strong biological imprint on surface water C and O cycles. By comparison, lower salinity surface waters of the Amundsen Sea ($S<33.5$ psu) showed a significantly lower O_2 *vs.* DIC slope (0.70 ± 0.02), as did regions with very high wind speeds (>20 m s^{-1}). This lower slope likely results from the effects of differential gas exchanges (see Section 4).

Beyond the strong CO_2–$\Delta O_2/Ar$ correlation we observed in Amundsen Sea surface waters, there were several other notable correlations among gas and hydrographic data in our high resolution underway data. DMS concentrations showed a significant negative correlation with pCO_2 and a positive correlation with $\Delta O_2/Ar$ (Tables 1 and 2). Underway Chl *a* fluorescence showed strong positive correlations with both $\Delta O_2/Ar$ and DMS, and a negative correlation with pCO_2 (Tables 1 and 2). Using discrete measurements from our 51 sampling stations, we found that the relative abundance of *P. antarctica* was positively correlated to surface DMS concentrations ($r=0.75$) and negatively correlated to pCO_2 ($r=-0.85$) across our survey region, providing further evidence that this species dominated much of the primary productivity and DMS(P) cycling in polynya surface waters. These correlations do not simply reflect a relationship of gas concentrations with total phytoplankton biomass, since the correlation coefficients for CO_2 and DMS with bulk Chl *a* ($r=-0.57$ and 0.5, respectively) were significantly lower for the station data than the correlations with relative *P. antarctica* abundance. Among the hydrographic variables we measured, salinity showed a relatively weak positive correlation with pCO_2 in polynya waters, while, SST showed a strong negative correlation with pCO_2 and positive correlations with both $\Delta O_2/Ar$ and DMS (Tables 1 and 2).

3.4. Sea–air gas fluxes

Sea–air gas fluxes varied substantially along our cruise track due to underlying variability in both wind speeds and surface ocean gas concentrations. Both DMS and CO_2 fluxes showed non-normal frequency distributions, with strong positive and negative skew, respectively. The mean DMS flux (calculated from 12.5 km binned

data) across the entire survey region was 23.1 μmol m^{-2} d^{-1}, with a median value of 7.3 μmol m^{-2} d^{-1}, and an inter-quartile range of 19.4 μmol m^{-2} d^{-1}. The mean CO_2 flux, derived from 12.5 km binned data, was −15.9 mmol m^{-2} d^{-1} (negative values imply flux into the ocean), with a median value and inter-quartile range of −2.9 and 13.8 mmol m^{-2} d^{-1}, respectively. Sea–air fluxes calculated exclusively for ice-free polynya waters were significantly higher than the survey averages, with values of 58.3 μmol DMS m^{-2} d^{-1} (IQR=67 μmol m^{-2} d^{-1}) and −41.9 mmol CO_2 m^{-2} d^{-1} (IQR= 38.9 mmol m^{-2} d^{-1}). For CO_2, variability in surface concentrations and wind speeds contributed about equally to the observed variability in fluxes (coefficient of variation=53% and 42% for wind speed and pCO_2, respectively). In contrast, variability in surface water DMS concentrations (coefficient of variation=150%) was the dominant source of DMS flux variability across our sampling transect.

4. Discussion

4.1. Comparison of the Amundsen Sea with other Southern Ocean waters

Relative to other Antarctic polynyas, such as those in the Ross and Weddell Seas, very little information is available on the biological, chemical, and physical dynamics of the Amundsen Sea polynyas. Comprehensive bathymetric data for this region has only been obtained in the past few years (Nitsche et al., 2007) and dominant circulation patterns are still being described (Payne et al., 2007; Thoma et al., 2008). Most oceanographic field studies in the Amundsen Sea have thus far focused on understanding the pathways of MDCW transport onto the continental shelf and the role of this warm water mass in basal ice sheet melting (Walker et al., 2007; Thoma et al., 2008; Jenkins et al., 2010; Wåhlin et al., 2010). By comparison, there are very few *in situ* data characterizing surface water biogeochemistry in this region. Using remote sensing data, Arrigo et al. (2012) described a strong seasonal cycle in sea ice cover and phytoplankton biomass in the Amundsen Sea that is generally consistent with that observed in other Antarctic polynyas (Arrigo and van Dijken, 2003). However, the rates of C-fixation inferred from satellite data appear to be higher in the Amundsen Sea polynyas than anywhere else in the Southern Ocean (Arrigo et al., 1998). *In situ* observations are critical to understand the factors driving high apparent productivity of the Amundsen Sea and the effect of biological productivity on surface water gas concentrations.

While the global pCO_2 database (Takahashi et al., 2010) includes unpublished measurements from the Amundsen sea, the DMS, and $\Delta O_2/Ar$ data presented here are, to our knowledge, the first of their kind available for this region. Our measurements provide a snap-shot of surface water gas concentrations during the peak and initial decline of the annual phytoplankton bloom. The pCO_2 drawdown and O_2 supersaturation we observed are among the largest reported for any oceanic waters, consistent with satellite-based estimates of exceptionally high productivity in this system. The minimum pCO_2 of the Amundsen Sea (~80 μatm) is lower than that reported for the Ross Sea (Bates et al., 1998; Sweeney et al., 2000; Tortell et al., 2011), with correspondingly higher biologically induced O_2 saturation. $\Delta O_2/Ar$ data have previously been used to infer rates of Southern Ocean net community production north of the sea ice zone (NCP; Reuer et al., 2007; Tortell and Long, 2009). However, the complex physical dynamics of the Amundsen Sea invalidate the assumptions needed for robust mixed layer NCP estimation. Weak vertical stratification and upwelling result in fluxes of low O_2 waters into the surface layer, which lead to underestimation of local NCP (Kaiser et al., 2005; Long et al., 2011), particularly in regions of MCDW upwelling in PIB and the AP. Additionally, the large-amplitude seasonal cycle invalidates the steady-state assumption used to simplify the mixed layer O_2 mass balance to estimate NCP. Our $\Delta O_2/Ar$ data can thus be used to qualitatively infer high NCP in the Amundsen Sea, but they do not yield robust quantitative estimates for this important biogeochemical parameter without detailed knowledge of physical dynamics (Long et al., 2011).

The DMS concentrations we measured across our survey region were also exceptional in terms of global distributions. The highest DMS concentration we observed in the PIP (~350 nM) is similar to the maximum value of ~300 nM reported in the recently updated global database of ~50,000 DMS measurements (http://saga.pmel.noaa.gov/dms/; note that our data will be made freely available on this server). One potential caveat is the possibility that we overestimated DMS concentrations due to cell lysis in the ship's underway sampling system. This would be particularly problematic in waters dominated by colonial *Phaeocystis*, which were observed across much of our study region. In previous work, we compared underway MIMS DMS measurements with discrete gas chromatographic (GC) measurements derived from Niskin bottle samples (Tortell et al., 2011). Our results show a strong correlation between the two measurements but a maximum positive offset of 20% in MIMS data, suggesting a small, but non-negligible, overestimation of DMS concentration in water dominated by colonial *Phaeocystis*. Despite this potential caveat, our observations of extraordinarily high DMS concentrations in the Amundsen Sea are consistent with previous GC-based results in the Ross Sea (*e.g.* Ditullio and Smith, 1995). Such extreme DMS concentrations have typically been excluded from large-scale data syntheses. For example, the DMS climatology of Lana et al. (2011) excludes all values above the 99.9 percentile (*i.e.* > ~150 nM) in order to avoid biases in the objective analysis. Our results indicate, however, that DMS concentrations well in excess of 100 nM are common in polynya waters (Fig. 7) and suggest that large-scale averaging of DMS data could lead to underestimates of surface DMS concentrations in the coastal Southern Ocean.

Our data do not allow us to explicitly separate the contribution of *in situ* water column DMS production from a potential ice-melt source. Trevena and Jones (2006) demonstrated elevated (~40 nM) DMS concentrations in low Chl *a* waters of the Antarctic sea ice zone, which they attributed to ice melt in the late spring/early summer (*i.e.* through late December). In our survey, an ice melt source was likely to be less proportionately important to the overall DMS distribution in the Amundsen Sea. Less than 1% of observations exhibited DMS > 20 nM and Chl *a* < 1 μg L^{-1}, and the highest DMS concentrations we observed (> 100 nM) were in the central waters of the PIP, far removed from the sea ice marginal zone. It thus appears that the water column DMS source likely dominated over an ice-melt source during the time of our survey. The ice-melt source may, however, be more significant earlier in the growing season.

4.2. Contribution of the Amundsen Sea to regional sea–air gas fluxes

As discussed recently by Arrigo et al. (2008), the 4° × 5° Takahashi et al. (2009) global pCO_2 climatology does not adequately resolve the contribution of Antarctic continental shelf waters to total oceanic sea–air fluxes. Arrigo et al. (2008) estimated that the Ross Sea alone accounted for ~25% of the total Southern Ocean CO_2 sink. In this system, maximum oceanic CO_2 uptake occurs in January–February, with values ranging from ~30 to 60 mmol CO_2 m^{-2} d^{-1}. In open polynya waters of the Amundsen Sea, we observed CO_2 fluxes of ~40 mmol m^{-2} d^{-1}, which were very similar to those of the Ross Sea. Taking the total surface area of the Amundsen Sea polynas to be ~15% of the area of the Ross Sea polynya (Arrigo and Van Dijken, 2007), and

assuming that these two regions exhibit comparable seasonality of sea–air gas fluxes, we estimate that the Amundsen Sea will account for roughly 4% (*i.e.* 15% of 25%) of total Southern Ocean CO_2 uptake as estimated by Takahashi et al. (2009). This simple calculation could be significantly refined by additional data documenting the seasonal and inter-annual variability of CO_2 fluxes in this region.

We can use a slightly different approach to roughly estimate the contribution of the Amundsen Sea to Southern Ocean DMS fluxes. To scale our measured flux estimates to a yearly value, we make the simplifying (and likely conservative) assumption that all of the annual DMS flux occurs over a period of two months in the open polynya waters when phytoplankton growth is most active. Assuming a mean polynya size of 50×10^3 km^2 for the AP and PIP combined (Arrigo and van Dijken, 2003) and an average sea–air flux of 58 μmol DMS m^{-2} d^{-1} over 60 days yields an annual flux of ~0.01 Tg yr^{-1}. This value represents approximately 10% of the Southern Ocean DMS flux between 70°S and 80°S as recently estimated by Lana et al. (2011), but less than 0.5% of total Southern Ocean flux (waters south of 50°S).

The calculation above does not include the potentially significant DMS fluxes from the sea ice zone. Relative to the open pelagic waters north of the sea ice zone, we measured elevated DMS concentrations in the sea ice domain of our survey area (Fig. 6F). The extent to which the pack ice acts as a DMS source to the atmosphere depends upon the rate of DMS production in both the ice-covered water column and in sea ice habitats, and on the flux resistance imposed by sea ice and snow. Recent work has demonstrated significant DMS fluxes from the multi-year sea ice zone in the Weddell Sea (Zemmelink et al., 2005) and similarly elevated fluxes may be associated with the pack ice of the Amundsen Sea. At present, however, it is difficult to quantify the contribution of the sea ice zone to sea–air DMS fluxes due to a lack of suitable gas exchange parameterizations. Nonetheless, we conclude that the Amundsen Sea polynyas and adjacent sea ice zone contribute significantly to regional DMS sea–air flux within the Southern Ocean, although perhaps not to the overall flux of this vast oceanic domain.

Accumulation rates of the DMS oxidation product methanosulfonic acid (MSA) in continental snow and ice have been linked to the temporal evolution of coastal Antarctic polynyas and used to assess sea ice extent (Curran et al., 2003; Rhodes et al., 2009). While a positive relationship between sea ice extent and MSA accumulation has been reported in the Indian sector of the Southern Ocean (Curran et al., 2003), snow data collected adjacent to the Ross Sea suggest a negative correlation between sea ice cover and MSA accumulation in nearby Antarctic snow (Rhodes et al., 2009). The link between polynya size and MSA accumulation in Antarctica snow was attributed by Rhodes et al. (2009) to pelagic production of DMS in open polynya waters of the Ross Sea dominated by *P. antarctica*. In contrast, Curran et al. (2003) attributed the positive correlation between sea ice extent and MSA deposition to DMS production by sea ice algae. Our results suggest that DMS concentrations and, presumably sea–air fluxes, are significantly higher in open polynya waters than in the adjacent pack ice (Fig. 6F). As a result, regional DMS fluxes from the Amundsen Sea, and hence MSA deposition on nearby continental surfaces, are likely to follow a pattern similar to the Ross Sea, with high values observed during years of high open water. Given the relatively short atmospheric life-time of DMS oxidation products (Berresheim et al., 1993), high coastal DMS fluxes (as measured in the Amundsen Sea) are likely to have a disproportionately large influence on long-term paleo records of marine biogenic sulfur (*e.g.* Legrand et al., 1991), making these regions significant beyond their contributions to overall Southern Ocean DMS fluxes.

4.3. Physical—biological interactions driving gas variability

In the Amundsen Sea, and other Antarctic polynyas, surface water gas distributions are strongly influenced by physical processes, including surface warming, localized upwelling, and sea ice melt. These processes affect mixed layer dynamics and control the availability of nutrients and light for phytoplankton growth. In the early spring, small-scale spatial variability in surface gases is likely to be minimal, presuming that deep winter mixing has homogenized tracer distributions. As sea ice clears, variability in surface gases is coupled to variability in ice distributions and mixed layer depths. In regions of shallow mixed layers, alleviation of light limitation results in enhanced primary productivity, pCO_2 drawdown, and O_2 accumulation (Sweeney et al., 2000). The influence of mixed layer depth on primary productivity can persist well into the summer growing season where nutrients remain plentiful in surface waters. Indeed, we saw an enhancement of surface water (~5 m) Chl *a* concentrations in regions of shallow mixed layers (Fig. 5), indicating the importance of mixing dynamics for phytoplankton biomass accumulation.

At the cold temperatures of the Antarctic region, seawater density is influenced foremost by salinity and secondarily by temperature. The surface salinity and temperature ranges we observed across surface waters of our survey region (~1.5 psu and ~3.5 °C; Fig. 2) would be sufficient to decrease seawater density by 1.2 and 0.18 kg m^{-3}, respectively, relative to subsurface water masses. These density changes are significant in relation to subsurface water mass variability in the Amundsen Sea (mean density at 150 m = 1028.11 ± 0.051 kg m^{-3}, n = 152), and large enough to drive mixed layer stratification ($\Delta\sigma_t$ criteria of 0.05–0.125 kg m^{-3}). The distribution of surface water pCO_2 and ΔO_2/Ar in temperature–salinity space is shown in Fig. 12.

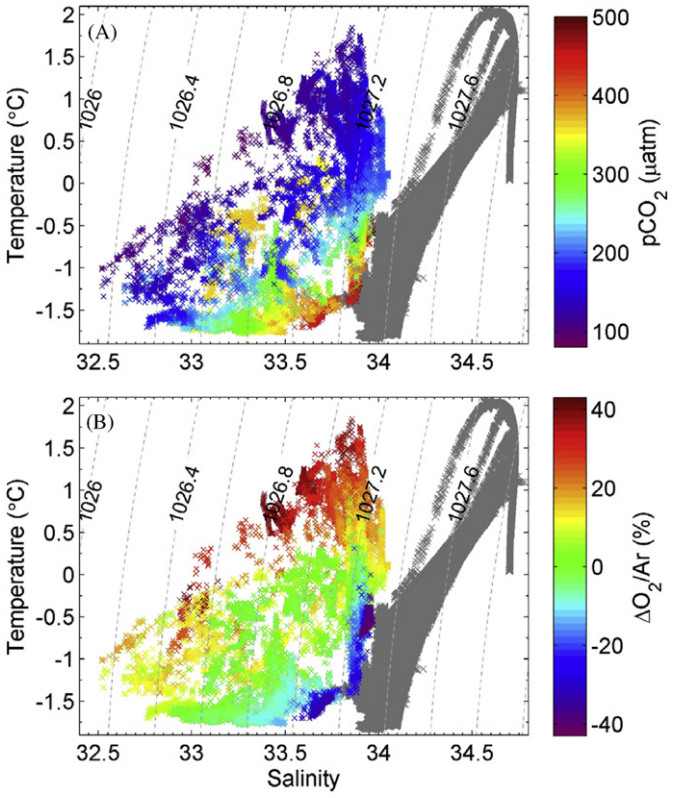

Fig. 12. Surface pCO_2 (A) and ΔO_2/Ar (B) as function of sea surface temperature and salinity. Gray symbols on the figure correspond to water masses >100 m deep where no gas data are available.

As can be seen in this figure, surface waters bearing a *T–S* signature close to that of the remnant Antarctic Winter Water (SST < 1.5, salinity ~34) show a strong net heterotrophic signature (*i.e.* $pCO_2 > 450$ µatm and $\Delta O_2/Ar < 0$), which is indicative of deep mixed layers and/or upwelling. As surface waters are modified, through both warming and freshening, the mixed layer becomes increasingly stratified and concomitantly accumulates a net productivity signal. This surface water productivity is evident in Fig. 12 as an increase in $\Delta O_2/Ar$ and pCO_2 drawdown along vectors of increasing SST and decreasing salinity. Examination of Fig. 12 shows that $\Delta O_2/Ar$ and pCO_2 exhibit a somewhat different behavior with respect to SST and salinity gradients. In particular, the $\Delta O_2/Ar$ distribution is asymmetric in *T–S* space, with high $\Delta O_2/Ar$ waters concentrated disproportionately in high SST regions (mostly in the PIP). Based on the anticipated relationship between mixed layer stratification and surface productivity, high $\Delta O_2/Ar$ would also be expected in low salinity waters (< 33.5), with shallow (< 20 m) mixed layer depths. Yet, these low salinity regions do not show particularly high $\Delta O_2/Ar$ despite extreme pCO_2 drawdown that is indicative of strong biological activity. As a result, the pCO_2 *vs.* $\Delta O_2/Ar$ relationship exhibits a significantly different slope in high and low salinity surface waters (Fig. 11).

The salinity dependence of the pCO_2–$\Delta O_2/Ar$ relationship (Fig. 11) cannot be explained by solubility changes or by melt-water dilution effects. The equilibrium O_2/Ar ratio is virtually constant (< 0.1% change) over the maximum range of salinity we observed (~34–32.6 psu), while CO_2 solubility changes by < 4%. Similarly, melt water dilution would only induce small changes in the seawater carbonate system relative to the large CO_2–$\Delta O_2/Ar$ ranges we observed. Assuming end member salinities of 34 and 6 psu for Antarctic surface water and ice-derived melt water, respectively (Dierssen et al., 2002), we calculate a relative contribution of 5% melt water into the mixed layer in the regions of minimum salinity, and a corresponding pCO_2 change of 14 µatm relative to unmodified Antarctic surface waters (DIC=2220, total alkalinity=2330; Jones et al., 2010). These effects are too small to account for the behavior seen in Fig. 11.

Unlike the thermodynamic effects describe above, sea–air fluxes have the capacity to introduce a large decoupling between O_2 and CO_2 in surface waters. While phytoplankton produce O_2 and consume DIC in a relatively constrained proportion (*i.e.* photosynthetic quotient) of ~1.2–1.4, gas exchange acts to obscure this biological C–O coupling since air–sea equilibration for O_2 is significantly faster than that of CO_2. Differential gas exchange can drive $\Delta O_2/Ar$ towards zero while CO_2 remains well below atmospheric equilibrium, resulting in a lower $\Delta O_2/Ar$ *vs.* pCO_2 slope as observed in Fig. 11A. The proportional effect of gas exchange on surface water gas inventories (and hence the O_2–CO_2 uncoupling) increases in shallow mixed layers (associated with fresher surface waters) and high wind speeds. In the Amundsen Sea, the influence of mixed layer depth on CO_2–O_2 coupling is manifested in the salinity-dependent slope of pCO_2 *vs.* $\Delta O_2/Ar$ (Fig. 11A). Superimposed on this is an effect of wind speed as shown in Fig. 11B. In regions of very high wind speed (> 20 m s^{-1}), located primarily along the ice edge in the AP, $\Delta O_2/Ar$ was nearly constant despite a large pCO_2 gradient. Our interpretation of this result is that gas exchange acted to ventilate excess O_2 in the mixed layer faster than the CO_2 re-equilibration time-scale. Although the data shown in Fig. 11 are derived from instantaneous, ship-based wind measurements, our argument would be more appropriately supported using winds averaged over the timescale of O_2 residence times in the mixed layer (~1–2 weeks). Unfortunately, climatological wind data (*e.g.* NCEP-NCAR reanalysis) have poor spatial resolution along the Antarctic margin so we have no robust way to estimate the wind history along our cruise track. Nonetheless, the results shown in Fig. 11B do provide a strong indication that high wind speeds and shallow mixed layers act to decouple O_2 and CO_2 from photosynthetic stoichiometry.

Although temperature-induced stratification plays a relatively weak role in controlling mixed layer dynamics in Antarctic polynyas, SST showed a strong correlation with surface water gas concentrations in the Amundsen Sea. This relationship likely reflects several underlying processes. First, increased SST can reflect the time-integrated effect of surface heat fluxes, with higher SST potentially indicating longer surface exposure. In this scenario, SST can serve as a physical 'clock', as warming accompanies the accumulation of a net production signal in surface waters. The distribution of pCO_2 and $\Delta O_2/Ar$ in the PIB region provides a potential example of this phenomenon. As shown in Fig. 9, we observed a strong productivity signal in the northeast corner of PIB (~102°W, 75′40°S; box A in the figure), in relatively high SST waters north of the MCDW upwelling/outflow zone. This spatial pattern may be explained by the prevailing surface currents in this region. As shown in Fig. 13, the general surface water circulation in PIB during our cruise was dominated by a clockwise gyre in the central bay, with low current speeds along the northeast coastal boundary where maximum $\Delta O_2/Ar$ was observed. Upwelling waters from underneath the PIG tongue (box B in Fig. 13) were transported into the gyre and distributed throughout the bay. Taking a value of ~200 km for the circumference of PIB, minimum travel times around the gyre would be approximately 4.5 days (assuming a current speed of 0.5 m s^{-1}), allowing for the accumulation of a net productivity signal. Waters transported into the northeast portion of the gyre encountered more sluggish circulation (due in part to lower wind speeds), resulting in increased surface residence times and greater accumulation of surface heat fluxes. This, in turn, would contribute to mixed layer stratification, providing a favorable light environment for phytoplankton to exploit the high macronutrient and Fe concentrations of recently upwelled waters.

The relationship between SST and $\Delta O_2/Ar$ may also partially reflect the influence of upwelling MCDW on phytoplankton productivity. This relatively warm water mass (*T*~1.1 °C) drives bottom melt of the glaciers (Jenkins et al., 2010; Jacobs et al., 2011), an important source of Fe (Gerringa et al., 2012) that fuels strong phytoplankton blooms. The supply of Fe through

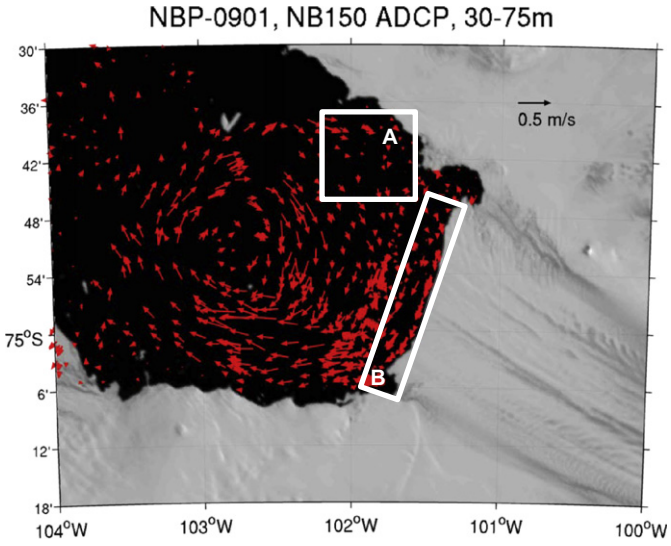

Fig. 13. Acoustic Doppler Current Profiler (ADCP) measurements showing mean surface currents (30–75 m) in Pine Island Bay during our survey period. Box A indicates the location of maximum $\Delta O_2/Ar$ and minimum pCO_2 observed in this region, while box B designates the region of inferred upwelling (see Fig. 9).

MCDW-driven glacier melt to the Amundsen Sea (with resulting concentrations approaching 1 nM; Gerringa et al., 2012) may explain the higher primary productivity and macronutrient consumption in this system relative to the Ross Sea, where background Fe levels are typically <0.4 nM (Coale et al., 2005). In particular, the observation that NO_3^- concentrations are depleted to very low levels in the offshore PIP region (Alderkamp et al., 2012), is consistent with enhanced Fe supply, possibly derived from MCDW melting of the PIG. Natural fertilization of the PIP may explain the extremely high apparent productivity ($\Delta O_2/Ar$ $\sim$40%) observed in this region, with high SST serving as a tracer for MCDW input.

A final consideration when interpreting the $\Delta O_2/Ar$–SST relationship is the direct effect of temperature on phytoplankton metabolic rates. The temperature-dependent maximum growth curve of Eppley (1972) predicts a 30% increase in phytoplankton growth rates over the SST range encountered in PIB. Recent experimental data have shown more modest (though statistically significant) temperature responses of phytoplankton assemblages in the Ross Sea (Rose et al., 2009). Although the exact magnitude of a temperature-dependent increase in phytoplankton growth rates is difficult to assess, it seems likely that the warming of surface waters may have acted to stimulate rates of photosynthetic C-fixation, contributing to the strong SST-dependence of surface water $\Delta O_2/Ar$.

4.4. DMS variability

The factors driving high DMS accumulation in the Amundsen Sea polynyas are likely similar to those operating in the Ross Sea. In this respect, the relative dominance of *P. antarctica* is expected to be a key factor since *Phaeocystis* species are prolific DMSP producers (Keller et al., 1989) and can catalyze the cellular cleavage of DMSP to DMS via the enzyme DMSP-lyase (Stefels and van Boekel, 1993; Stefels and Dijkhuizen, 1996). In the Amundsen Sea, *P. antarctica* dominates the phytoplankton assemblages during the later growth season, even under relatively stratified mixed layer conditions that are believed to favor diatoms in the Ross Sea (Arrigo et al., 2000). *P. antarctica* growth under such stratified summer conditions is particularly significant in the context of DMS production, given the potential role of DMS(P) as an anti-oxidant employed to detoxify O_2 radicals produced by excess irradiance and/or Fe limitation (Sunda et al., 2002). Enhanced mixed layer stratification results in increased irradiance levels, while Fe concentrations as low as $\sim$0.1 nM were observed towards the end of our cruise (Gerringa et al., 2012). Alderkamp et al. (2012) reported evidence for Fe stress in Amundsen Sea *P. antarctica* assemblages based on shifts in photosynthetic pigment signatures, even though variable fluorescence (F_v/F_m) data suggested that *P. antarctica* did not experience extreme Fe limitation. We suggest that elevated DMS(P) production by *P. antarctica* during late summer blooms serves as a mechanism to alleviate the physiological effects of low Fe and high light as observed in laboratory culture experiments (Stefels and Van Leeuwe, 1998).

Full understanding of DMS dynamics in the Amundsen Sea requires information on all of the production and loss terms in the mixed layer. In addition to the direct production from *P. antarctica* and other phytoplankton taxa, a significant fraction of the mixed layer DMS pool is likely derived from the bacterial metabolism of dissolved DMSP (Kiene and Linn, 2000; Kiene et al., 2000), which is released into the water column through a variety of processes including phytoplankton exudation, zooplankton grazing, and viral lysis (Stefels et al., 2007). Recent work in the Ross Sea has demonstrated very high rates of bacterial DMS consumption, particularly during the later summer growth period (del Valle et al., 2009). Summertime bacterial DMS consumption in this system far exceeds the loss terms due to photo-oxidation and sea–air flux and acts to limit the accumulation of DMS in the late summer polynya (del Valle et al., 2009). Unfortunately, there are no relevant data on DMS production/consumption rates in the mixed layer for our Amundsen Sea cruise. Nonetheless, it clear that overall DMS production rates must significantly exceed DMS loss rates in order to accumulate mixed layer concentrations in excess of 100 nM. The potential for high DMS production and consumption terms likely drives the heterogeneous surface water distributions and small-scale patchiness of this gas in the Amundsen Sea.

Rapid microbial cycling may help explain differences in the observed spatial distribution of DMS relative to CO_2 and $\Delta O_2/Ar$. In PIB, we observed maximum DMS concentrations that were spatially segregated from maximum $\Delta O_2/Ar$ and minimum pCO_2 (Fig. 9). Given the general clockwise circulation pattern in the bay (Fig. 13), it is conceivable that DMS production was stimulated at the beginning of phytoplankton blooms adjacent to the upwelling zone, but subsequent bacterial consumption limited DMS accumulation as the water circulated around the gyre acquiring a strong signature of net community production (*i.e.* high $\Delta O_2/Ar$, low pCO_2). Testing this hypothesis requires direct measurements of DMS production and consumption rates in the mixed layer, ideally using a Lagrangian approach to track individual water masses and separate the spatial and temporal components of the observed variability.

4.5. Scale-dependent spatial variability

Several recent articles have quantified the length scales of surface gas and hydrographic variability in the Ross Sea using high spatial resolution measurements (Hales and Takahashi, 2004; Tortell et al., 2011). These analyses have demonstrated that much of the variability in that system is present at scales less than $\sim$10 km. Such spatial analyses are particularly challenging for our Amundsen Sea data given the convoluted nature of our sampling transects and the potential for aliasing temporal and spatial variability along the cruise track. Nonetheless, we have computed simple auto-correlation functions for two linear transects in our survey (Fig. 14). One of these transects bisected PIB, starting at the face of the PIG and moving towards the northwest.

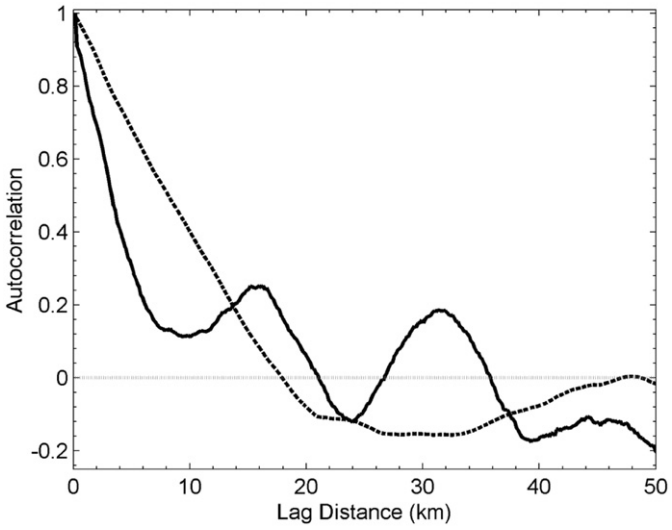

Fig. 14. Autocorrelation functions for $\Delta O_2/Ar$ data measured along a transect through PIB and along the sea ice edge in the Amundsen polynya. For both sets of measurements, the decorrelation length scale (i.e. first zero crossing of the ACF) is $\sim$20 km.

The other transect was sampled along the face of the marginal ice zone in the southwestern AP. For both of these transects, the auto-correlation functions show a rapid decrease on spatial scales of <10 km, and a decorrelation length scale (*i.e.* the position where the auto-correlation goes to zero) of $\sim$20 km. This result highlights the sub-mesoscale variability of surface gases in the Amundsen Sea and suggests that such fine-scale heterogeneity is characteristic of many Antarctic polynyas.

A variety of mechanisms likely drive the observed fine-scale spatial variability we observed. During the early phytoplankton growth season, variance in surface gas distributions is initially driven by the underlying distribution of limiting resources (*e.g.* light and possibly Fe). Primary productivity responds to this variability, generating gradients in gas concentrations at scales over which MLD and limiting nutrients vary. Mixed layer depths can vary over large spatial scales due to ice melt contributions to surface waters. In addition, horizontal advection has been shown to influence mixed layer dynamics on sub-mesoscales by causing lighter water to flow over more dense water, flattening isopycnals (Boccaletti et al., 2007; Fox-Kemper et al., 2008). As the phytoplankton bloom progresses, stirring by eddies operates on horizontal gradients, causing variance to propagate to smaller spatial scales (Rhines, 1986). Similarly, Ekman advection has been shown to be important for structuring pCO_2 distributions during the spring bloom in the Ross Sea (Long et al., 2012). These processes are likely to operate in the Amundsen Sea where strong horizontal density gradients exist. Spatial variability in the supply of Fe to surface waters appears to be controlled to a large extent, by localized MCDW-derived glacial melt water inputs (Gerringa et al., 2012). Furthermore, ice melt may contain Fe derived from spatially heterogeneous eolian deposition. A variety of mechanisms thus exist to create small-scale variability in mixed layer dynamics and Fe supply. Our results underscore the need for high resolution underway analysis to fully describing the spatial distribution of surface water gases in the Amundsen Sea and other Antarctic continental shelf waters.

5. Conclusions and future prospects

The pCO_2, $\Delta O_2/Ar$, and DMS concentrations we observed in surface waters of the Amundsen Sea indicate that this system has the potential for exceptionally high biological productivity, consistent with remote sensing observations. A strong biological imprint in surface waters is evident from the tight correlation between Chl *a* and gas concentrations, and a stoichiometric relationship between CO_2 and $\Delta O_2/Ar$ that is consistent with photosynthetic production in the mixed layer. Despite the strong influence of biological processes on surface gas distributions, hydrographic variability resulting from surface warming, upwelling and sea ice melt also imposes significant heterogeneity in surface gases. Moreover, sea–air exchange likely plays an important role in determining CO_2/O_2 ratios in the mixed layer. Upwelling of MCDW appears to be a significant driver of the exceptionally high productivity in the Amundsen Sea polynyas, likely due to the high glacially-derived Fe concentrations of this water mass. The extraordinarily high DMS levels we observed may result from the growth of *P. antarctica* under conditions of oxidative stress imposed by high irradiance in shallow mixed layers and possibly by the onset of Fe limitation. Complex microbial cycling likely explains the high spatial variability of DMS in the Amundsen Sea.

Future studies should attempt to increase the temporal coverage of gas measurements in the Amundsen Sea to constrain the annual sea–air fluxes of CO_2 and DMS in this system and its relative contribution to total Southern Ocean gas cycling. For DMS, more information is also needed on the underlying microbial production and consumption terms. In this respect, high resolution underway surveys coupled with focused process studies (Asher et al., 2011) will be important. It will also be important to explore the influence of surface water hydrography on surface gas concentrations in the Amundsen Sea (and other Antarctic polynya waters) over interannual timescales. In light of anticipated climate changes over the coming century and the attendant shifts in sea ice distributions and biological community structure (Sarmiento et al., 1998), hydrographic influences on surface gases could drive biogeochemical climate feedback processes as predicted in recent modeling studies (Cameron-Smith et al., 2011).

Acknowledgments

This work was supported by the US National Science Foundation, Office of Polar Programs (Grant # ANT0732535 to KRA), and funding from the Natural Sciences and Engineering Research Council of Canada (PDT). We thank the Captain and crew of the RVIB *Nathanial B. Palmer* for logistical assistance, as well as the entire DynaLiFe science team for support at sea and valuable intellectual input. Quality-controlled pCO_2 data from the equilibrator on the NB Palmer were provided courtesy of Taro Takahashi and the Lamont Doherty Earth Observatory CO_2 group.

References

Alderkamp, A.C., Mills, M.M., van Dijken, G.L., Laan, P., Thuroczy, C.E., Gerringa, L., de Baar, H.J.W., Payne, C., Tortell, P., Visser, R.J.W., Buma, A.G.J., Arrigo, K.R., 2012. Iron from melting glaciers fuels phytoplankton blooms in Amundsen Sea (Southern Ocean); phytoplankton characteristics and productivity. Deep-Sea Res. II 71–76, 32–48.

Arrigo, K.R., Lowry, K., van Dijken, G., 2012. Annual changes in sea ice and phytoplankton in polynyas of the Amundsen Sea, Antarctica. Deep-Sea Res. II 71–76, 5–15.

Arrigo, K.R., DiTullio, G.R., Dunbar, R.B., Robinson, D.H., VanWoert, M., Worthen, D.L., Lizotte, M.P., 2000. Phytoplankton taxonomic variability in nutrient utilization and primary production in the Ross Sea. J. Geophys. Res.-Oceans 105 (C4), 8827–8845.

Arrigo, K.R., van Dijken, G., Long, M., 2008. Coastal Southern Ocean: a strong anthropogenic CO_2 sink. Geophys. Res. Lett. 35, 21.

Arrigo, K.R., van Dijken, G.L., 2003. Phytoplankton dynamics within 37 Antarctic coastal polynya systems. J. Geophys. Res.-Oceans 108 (C8).

Arrigo, K.R., Van Dijken, G.L., 2007. Interannual variation in air–sea CO_2 flux in the Ross Sea, Antarctica: a model analysis. J. Geophys. Res.-Oceans 112 (C3).

Arrigo, K.R., Worthen, D., Schnell, A., Lizotte, M.P., 1998. Primary production in Southern Ocean waters. J. Geophys. Res.-Oceans 103 (C8), 15587–15600.

Asher, E.C., Dacey, J.W.H., Mills, M.M., Arrigo, K.R., Tortell, P.D., 2011. High concentrations and turnover rates of DMS, DMSP and DMSO in Antarctic sea ice. Geophys. Res. Lett. 38 (23), L23609, doi:10.1029/2011GL049712.

Bates, N.R., Hansell, D.A., Carlson, C.A., Gordon, L.I., 1998. Distribution of CO_2 species, estimates of net community production, and air–sea CO_2 exchange in the Ross Sea polynya. J. Geophys. Res.-Oceans 103 (C2), 2883–2896.

Bates, T.S., Lamb, B.K., Guenther, A., Dignon, J., Stoiber, R.E., 1992. Sulfur emissions to the atmosphere from natural sources. J. Atmos. Chem. 14 (1), 315–337.

Berresheim, H., Eisele, F.L., Tanner, D.J., McInnes, L.M., Ramsey-Bell, D.C., Covert, D.S., 1993. Atmospheric sulfur chemistry and cloud condensation nuclei (CCN) concentrations over the northeastern Pacific coast. J. Geophys. Res. 98 (D7). (12701–12712, 12711).

Boccaletti, G., Ferrari, R., Fox-Kemper, B., 2007. Mixed layer instabilities and restratification. J. Phys. Oceanogr. 37 (9), 2228–2250.

Bopp, L., Boucher, O., Aumont, O., Belviso, S., Dufresne, J.L., Pham, M., Monfray, P., 2004. Will marine dimethylsulfide emissions amplify or alleviate global warming? A model study. Can. J. Fish. Aquat. Sci. 61 (5), 826–835.

Boyd, P.W., 2002. Environmental factors controlling phytoplankton processes in the Southern Ocean. J. Phycol. 38 (5), 844–861.

Cameron-Smith, P., Elliott, S., Maltrud, M., Erickson, D., Wingenter, O., 2011. Changes in dimethyl sulfide oceanic distribution due to climate change. Geophys. Res. Lett. 38 (7), L07704.

Cavalieri, D., Thorsten, M., Comiso, J., 2004. AMSR-E/Aqua Daily L3 12.5 km Brightness Temperature, Sea Ice Concentration, & Snow Depth Polar Grids V002. National Snow and Ice Data Center. Digital Media, Boulder, Colorado USA (updated daily).

Charlson, R.J., Lovelock, J.E., Andreae, M.O., Warren, S.G., 1987. Oceanic phytoplankton, atmospheric sulfur, cloud albedo and climate. Nature 326 (6114), 655–661.

Coale, K.H., Gordon, R.M., Wang, X.J., 2005. The distribution and behavior of dissolved and particulate iron and zinc in the Ross Sea and Antarctic circumpolar current along 170 degrees W. Deep-Sea Res. I 52 (2), 295–318.
Craig, H., Hayward, T., 1987. Oxygen supersaturation in the ocean—biological *versus* physical contributions. Science 235 (4785), 199–202.
Curran, M.A.J., van Ommen, T.D., Morgan, V.I., Phillips, K.L., Palmer, A.S., 2003. Ice core evidence for Antarctic sea ice decline since the 1950s. Science 302 (5648), 1203.
del Valle, D.A., Kieber, D.J., Toole, D.A., Brinkley, J., Kiene, R.P., 2009. Biological consumption of dimethylsulfide (DMS) and its importance in DMS dynamics in the Ross Sea, Antarctica. Limnol. Oceanogr. 54 (3), 785–798.
Dierssen, H.M., Smith, R.C., Vernet, M., 2002. Glacial meltwater dynamics in coastal waters west of the Antarctic Peninsula. Proc. Natl. Acad. Sci. USA 99 (4), 1790.
Ditullio, G.R., Smith, W.O., 1995. Relationship between dimethylsulfide and phytoplankton pigment concentrations in the Ross Sea, Antarctica. Deep-Sea Res. I 42 (6), 873–892.
DiTullio, G.R., Smith, W.O., 1996. Spatial patterns in phytoplankton biomass and pigment distributions in the Ross Sea. J. Geophys. Res.-Oceans 101 (C8), 18467–18477.
Dunbar, R.B., Leventer, A.R., Mucciarone, D.A., 1998. Water column sediment fluxes in the Ross Sea, Antarctica: atmospheric and sea ice forcing. J. Geophys. Res.-Oceans 103 (C13), 30741–30759.
Eppley, R.W., 1972. Temperature and phytoplankton growth in the sea. Fish. Bull. 70 (4), 1063–1085.
Fox-Kemper, B., Ferrari, R., Hallberg, R., 2008. Parameterization of mixed layer eddies. Part I: theory and diagnosis. J. Phys. Oceanogr. 38 (6), 1145–1165.
Gerringa, L.J.A., Alderkamp, A.C., Laan, P., Thuróczy, C.E., de Baar, H.J.W., Mills, M.M., van Dijken, G., van Haren, H., Arrigo, K.R., 2012. Iron from melting glaciers fuels the phytoplankton blooms in Amundsen Sea (Southern Ocean): iron biogeochemistry. Deep-Sea Res. II 71–76, 16–31.
Gibson, J.A.E., Trull, T.W., 1999. Annual cycle of fCO_2 under sea-ice and in open water in Prydz Bay, East Antarctica. Mar. Chem. 66 (3–4), 187–200.
Hales, B., Takahashi, T., 2004. High-resolution biogeochemical investigation of the Ross Sea, Antarctica, during the AESOPS (U.S. JGOFS) Program. Global Biogeochem. Cycles 18 (3), 24.
Jacobs, S.S., 2004. Bottom water production and its links with the thermohaline circulation. Antarct. Sci. 16 (4), 427–437.
Jacobs, S.S., Giulivi, C.F., 2010. Large multidecadal salinity trends near the Pacific–Antarctic continental margin. J. Clim. 23 (17), 4508–4524.
Jacobs, S.S., Jenkins, A., Giulivi, C.F., Dutrieux, P., 2011. Stronger ocean circulation and increased melting under Pine Island Glacier ice shelf. Nature Geosci. 4 (8), 519–523.
Jenkins, A., Dutrieux, P., Jacobs, S.S., McPhail, S.D., Perrett, J.R., Webb, A.T., White, D., 2010. Observations beneath Pine Island Glacier in West Antarctica and implications for its retreat. Nat. Geosci. 3 (7), 468–472.
Jones, E.M., Bakker, D.C.E., Venables, H.J., Whitehouse, M.J., Korb, R.E., Watson, A.J., 2010. Rapid changes in surface water carbonate chemistry during Antarctic Sea ice melt. Tellus B 62B, 621–635.
Kaiser, J., Reuer, M.K., Barnett, B., Bender, M.L., 2005. Marine productivity estimates from continuous O_2/Ar ratio measurements by membrane inlet mass spectrometry. Geophys. Res. Lett. 32 (19), L19605. doi:10.1029/2005GL023459.
Keller, M.D., Bellows, W.K., Guillard, R.R.L., 1989. Dimethyl sulfide production in marine phytoplankton. Biogenic sulfur in the environment. ACS Symp. Ser. 393, 167–182.
Kiene, R.P., Kieber, D.J., Slezak, D., Toole, D.A., del Valle, D.A., Bisgrove, J., Brinkley, J., Rellinger, A., 2007. Distribution and cycling of dimethylsulfide, dimethylsulfoniopropionate, and dimethylsulfoxide during spring and early summer in the Southern Ocean south of New Zealand. Aquat. Sci. 69 (3), 305–319.
Kiene, R.P., Linn, L.J., 2000. The fate of dissolved dimethylsulfoniopropionate (DMSP) in seawater: tracer studies using S-35-DMSP. Geochim. Cosmochim. Acta 64 (16), 2797–2810.
Kiene, R.P., Linn, L.J., Bruton, J.A., 2000. New and important roles for DMSP in marine microbial communities. J. Sea Res. 43 (3–4), 209–224.
Lana, A., Bell, T.G., Simo, R., Vallina, S.M., Ballabrera-Poy, J., Kettle, A.J., Dachs, J., Bopp, L., Saltzman, E.S., Stefels, J., 2011. An updated climatology of surface dimethlysulfide concentrations and emission fluxes in the global ocean. Global Biogeochem. Cycles, 25.
Laws, E.A., 1991. Photosynthetic quotients, new production and net community production in the open ocean. Deep-Sea Res. I 38 (1), 143–167.
Legrand, M., Fenietsaigne, C., Saltzman, E.S., Germain, C., Barkov, N.I., Petrov, V.N., 1991. Ice-core record of oceanic emissions of dimethylsulfide during the last climate cycle. Nature 350 (6314), 144–146.
Long, M.C., Thomas, L.N., Dunbar, R.B., 2012. Control of phytoplankton bloom inception in the Ross Sea, Antarctica, by Ekman restratification. Global Biogeochemical Cycles 26, Gb1006, doi:10.1029/2010gb003982.
Long, M.C., Dunbar, R.B., Tortell, P.D., Smith, W.O., Mucciarone, D.A., DiTullio, G.R., 2011. Vertical structure, seasonal drawdown, and net community production in the Ross Sea, Antarctica. J. Geophys. Res.-Oceans 116, 19.
Mackey, M.D., Mackey, D.J., Higgins, H.W., Wright, S.W., 1996. CHEMTAX-A program for estimating class abundances from chemical markers: application to HPLC measurements of phytoplankton. Mar. Ecol. Prog. Ser. 14 (1–3), 265–283.
Marinov, I., Gnanadesikan, A., Toggweiler, J.R., Sarmiento, J.L., 2006. The Southern Ocean biogeochemical divide. Nature 441 (7096), 964–967.
Nitsche, F.O., Jacobs, S.S., Larter, R.D., Gohl, K., 2007. Bathymetry of the Amundsen Sea continental shelf: implications for geology, oceanography, and glaciology. Oceanography 9310, 9315.
Payne, A.J., Holland, P.R., Shepherd, A.P., Rutt, I.C., Jenkins, A., Joughin, I., 2007. Numerical modeling of ocean–ice interactions under Pine Island Bay's ice shelf. J. Geophys. Res. 112 (C10), C10019.
Reuer, M.K., Barnett, B.A., Bender, M.L., Falkowski, P.G., Hendricks, M.B., 2007. New estimates of Southern Ocean biological production rates from O_2/Ar ratios and the triple isotope composition of O_2. Deep-Sea Res. I 54 (6), 951–974.
Rhines, P.B., 1986. Vorticity dynamics of the oceanic general circulation. Annu Rev. Fluid Mech. 18 (1), 433–497.
Rhodes, R.H., Bertler, N.A.N., Baker, J.A., Sneed, S.B., Oerter, H., Arrigo, K.R., 2009. Sea ice variability and primary productivity in the Ross Sea, Antarctica, from methylsulphonate snow record. Geophys. Res. Lett. 36 (10), L10704.
Rose, J.M., Feng, Y., DiTullio, G.R., Dunbar, R.B., Hare, C.E., Lee, P.A., Lohan, M., Long, M., Smith, W.O., Sohst, B., 2009. Synergistic effects of iron and temperature on Antarctic phytoplankton and microzooplankton assemblages. Biogeosciences 6 (12), 3131–3147.
Saltzman, E.S., King, D.B., Holmen, K., Leck, C., 1993. Experimental determination of the diffusion coefficient of dimethylsulfide in water. J. Geophys. Res. 98 (C9). (16481–16416, 16486).
Sarmiento, J.L., Hughes, T.M.C., Stouffer, R.J., Manabe, S., 1998. Simulated response of the ocean carbon cycle to anthropogenic climate warming. Nature 393 (6682), 245–249.
Sedwick, P.N., DiTullio, G.R., 1997. Regulation of algal blooms in Antarctic shelf waters by the release of iron from melting sea ice. Geophys. Res. Lett. 24 (20), 2515–2518.
Simo, R., 2004. From cells to globe: approaching the dynamics of DMS(P) in the ocean at multiple scales. Can. J. Fish. Aquat. Sci. 61 (5), 673–684.
Smith, W.O., Marra, J., Hiscock, M.R., Barber, R.T., 2000. The seasonal cycle of phytoplankton biomass and primary productivity in the Ross Sea, Antarctica. Deep-Sea Res. II 47 (15–16), 3119–3140.
Stefels, J., Dijkhuizen, L., 1996. Characteristics of DMSP-lyase in *Phaeocystis* sp. (Prymnesiophyceae). Mar. Ecol.-Prog. Ser. 131 (1–3), 307–313.
Stefels, J., Steinke, M., Turner, S., Malin, G., Belviso, S., 2007. Environmental constraints on the production and removal of the climatically active gas dimethylsulphide (DMS) and implications for ecosystem modelling. Biogeochemistry 83 (1–3), 245–275.
Stefels, J., van Boekel, W.H.M., 1993. Production of DMS from dissolved DMSP in axenic cultures of the marine phytoplankton species *Phaeocystis* sp. Mar. Ecol. Prog. Ser. 97, 11–18.
Stefels, J., Van Leeuwe, M.A., 1998. Effects of iron and light stress on the biochemical composition of Antarctic *Phaeocystis* sp. (Prymnesiophyceae). I. Intracellular DMSP concentrations. J. Phycol. 34 (3), 486–495.
Sunda, W., Kieber, D.J., Kiene, R.P., Huntsman, S., 2002. An antioxidant function for DMSP and DMS in marine algae. Nature 418 (6895), 317–320.
Sweeney, C., 2003. The annual cycle of surface CO_2 and O_2 in the Ross Sea: a model for gas exchange on the continental shelves of Antarctica. In: DiTullio, G.R., Dunbar, R.B. (Eds.), Biogeochemistry of the Ross Sea, Antarctic Research Series, vol. 78, pp. 295–312.
Sweeney, C., Hansell, D.A., Carlson, C.A., Codispoti, L.A., Gordon, L.I., Marra, J., Millero, F.J., Smith, W.O., Takahashi, T., 2000. Biogeochemical regimes, net community production and carbon export in the Ross Sea, Antarctica. Deep-Sea Res. II 47 (15–16), 3369–3394.
Takahashi, T., Sweeney, C., Sutherland, S.C., Chipman, D.W., Goddard, J., Rubin, S.I., 2000. Method of Underway pCO_2 Measurements in Surface Waters and the Atmosphere During the Aesops Expeditions, 1996–1998 in the Pacific Sector of the Southern Ocean and the Ross Sea. US JGOFS Data Center, Woods Hole Oceanographic Institution, Woods Hole, MA.
Takahashi, T., Sutherland, S.C., Wanninkhof, R., Sweeney, C., Feely, R.A., Chipman, D.W., Hales, B., Friederich, G., Chavez, F., Sabine, C., 2009. Climatological mean and decadal change in surface ocean pCO_2, and net sea–air CO_2 flux over the global oceans. Deep-Sea Res. II 56 (8–10), 554–577.
Takahashi, T., Sutherland, S.C., Kozyr, A., 2010. Global Ocean Surface Water Partial Pressure of CO_2 Database: Measurements Performed During 1957–2009 (Version 2009). ORNL/CDIAC-152, NDP-088(V2009). Carbon Dioxide Information Analysis Center, Oak Ridge National Laboratory, U.S. Department of Energy, Oak Ridge, Tennessee. doi:10.3334/CDIAC/otg.ndp088(V2009).
Thoma, M., Jenkins, A., Holland, D., Jacobs, S., 2008. Modelling circumpolar deep water intrusions on the Amundsen Sea continental shelf, Antarctica. Geophys. Res. Lett. 35. (10.1029).
Thomas, M.A., Suntharalingam, P., Pozzoli, L., Rast, S., Devasthale, A., Kloster, S., Feichter, J., Lenton, T.M., 2010. Quantification of DMS aerosol–cloud–climate interactions using the ECHAM5-HAMMOZ model in a current climate scenario. Atmos. Chem. Phys. 10, 7425–7438.
Thomas, R., Rignot, E., Casassa, G., Kanagaratnam, P., Acuña, C., Akins, T., Brecher, H., Frederick, E., Gogineni, P., Krabill, W., 2004. Accelerated sea-level rise from West Antarctica. Science 306 (5694), 255.
Tortell, P.D., 2005. Dissolved gas measurements in oceanic waters made by membrane inlet mass spectrometry. Limnol. Oceanogr.-Methods 3, 24–37.
Tortell, P.D., Guéguen, C., Long, M.C., Payne, C.D., Lee, P., DiTullio, G.R., 2011. Spatial variability and temporal dynamics of surface water pCO_2, DO_2/Ar and dimethylsulfide in the Ross Sea, Antarctica. Deep-Sea Res. I 58 (3), 241–259.
Tortell, P.D., Long, M.C., 2009. Spatial and temporal variability of biogenic gases during the Southern Ocean spring bloom. Geophys. Res. Lett. 36, L01603. doi:10.1029/2008GL035819.

Trevena, A.J., Jones, G.B., 2006. Dimethylsulphide and dimethylsulphoniopropionate in Antarctic sea ice and their release during sea ice melting. Mar. Chem. 98 (2–4), 210–222.
Vlahos, P., Monahan, E.C., 2009. A generalized model for the air–sea transfer of dimethyl sulfide at high wind speeds. Geophys. Res. Lett. 36, L21605. doi:10.1029/2009GL040695.
Wåhlin, A.K., Yuan, X., Björk, G., Nohr, C., 2010. Inflow of warm circumpolar deep water in the central Amundsen shelf. J. Phys. Oceanogr. 40 (6), 1427–1434.
Walker, D.P., Brandon, M.A., Jenkins, A., Allen, J.T., Dowdeswell, J.A., Evans, J., 2007. Oceanic heat transport onto the Amundsen Sea shelf through a submarine glacial trough. Geophys. Res. Lett. 34 (L02602), 1–4.
Wanninkhof, R., 1992. Relationship between wind-speed and gas exchange over the ocean. J. Geophys. Res.-Oceans 97 (C5), 7373–7382.
Weiss, R.F., 1974. Carbon dioxide in water and seawater: the solubility of a non-ideal gas. Mar. Chem. 2 (3), 203–215.
Welschmeyer, N.A., 1994. Fluorometric analysis of chlorophyll a in the presence of chlorophyll b and pheopigments. Limnol. Oceanogr. 39 (8), 1985–1992.
Zemmelink, H.J., Houghton, L., Dacey, J.W.H., Worby, A.P., Liss, P.S., 2005. Emission of dimethylsulfide from Weddell Sea leads. Geophys. Res. Lett. 32 (2005), L23610. doi:10.1029/2005GL024242.